Technical Report:

Flow Past a Descending Balloon

NASA Award NAG5-5292

Period: 18 May 2000 - 30 November 2001

Submitted to:

Balloon Program Office
NASA/GSFC/WFF
Wallops Island, VA

Planetary Aerobot Program
NASA/JPL
Pasadena, CA

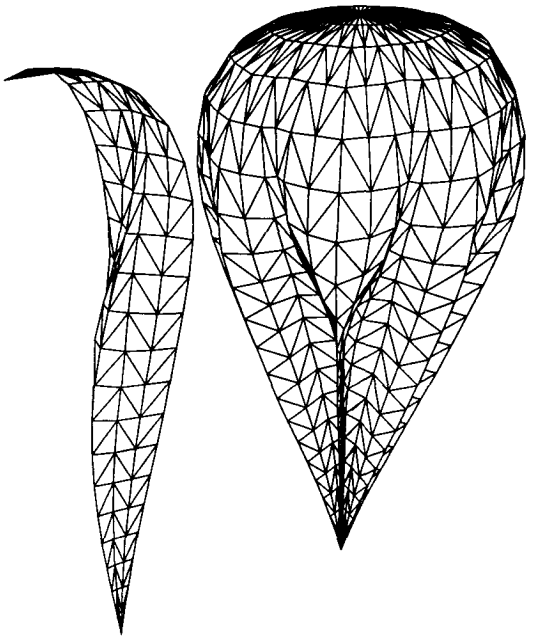

Frank Baginski, Principal Investigator

Department of Mathematics
The George Washington University
Washington, DC 20052

31 December 2001

Abstract

In this report, we present our findings related to aerodynamic loading of partially inflated balloon shapes. This report will consider aerodynamic loading of partially inflated inextensible natural shape balloons and some relevant problems in potential flow. For the axisymmetric modeling, we modified our Balloon Design Shape Program (BDSP) to handle axisymmetric inextensible ascent shapes with aerodynamic loading. For a few simple examples of two dimensional potential flows, we used the Matlab PDE Toolbox. In addition, we propose a model for aerodynamic loading of strained energy minimizing balloon shapes with lobes. Numerical solutions are presented for partially inflated strained balloon shapes with lobes and no aerodynamic loading.

Flow Past a Descending Balloon

Frank Baginski
Department of Mathematics
The George Washington University
Washington, DC 20052

31 December 2001

Contents

List of Figures

List of Tables

Chapter 1

Aerodynamic loading

1.1 Aerodynamic loading of natural shape balloons

1.1.1 Background

The equations for a natural balloon shape were first derived by researchers at the University of Minnesota (see [1]). A derivation of these equations is presented in [7, Sec. V]. Extensive computations were carried out on a digital computer by Smalley (see, e.g., [15]–[16]). Axisymmetric ascent shapes were considered in [3]. We follow the approach in [3], modeling the balloon as an axisymmetric inextensible membrane. However, in the present work, we add caps and aerodynamic forces to the model for axisymmetric natural shape balloons. Balloons constructed from a single shell, but with sections of different material properties can also be considered. We begin with some notation and then provide some physical justification for the governing equations.

1.1.2 Equilibrium equations

Since we seek axisymmetric solutions, we need to find a generating curve $s \to (z(s), r(s))$, where s is the arc-length. Let ℓ_d be the total length of the generating curve. We can express the solution as $\mathbf{x}(s,\phi)$ (see Figure 1.1), where $s \in [0,\ell_d]$, $\phi \in [0,2\pi]$, and

$$\begin{aligned} \mathbf{x}(s,\phi) &= r(s)\mathbf{e}_1(\phi) + z(s)\mathbf{e}_3(\phi), \\ \mathbf{e}_1(\phi) &= \cos\phi\mathbf{i} + \sin\phi\mathbf{j}, \\ \mathbf{e}_3(\phi) &= \mathbf{k}. \end{aligned}$$

It is useful to define $\mathbf{e}_2(\phi)$ to be the unit vector which completes the right-hand triad $\{\mathbf{e}_1(\phi), \mathbf{e}_2(\phi), \mathbf{e}_3(\phi)\}$,

$$\mathbf{e}_2(\phi) = \mathbf{e}_3(\phi) \times \mathbf{e}_1(\phi) = -\sin\phi\mathbf{i} + \cos\phi\mathbf{j}. \tag{1.1}$$

The balloon's shape is defined by the parametrized surface,

$$S = \{\mathbf{x}(s,\phi) \mid s \in [0,\ell_d], \phi \in [0,2\pi]\}. \tag{1.2}$$

At each point along the curve, $s \to \mathbf{x}(s,\phi)$, the tangent vector is given by

$$\mathbf{a}(s,\phi) = \frac{\partial \mathbf{x}}{\partial s}(s,\phi) = \sin\theta(s)\mathbf{e}_1(\phi) + \cos\theta(s)\mathbf{e}_3(\phi), \tag{1.3}$$

where $\theta(s)$ is the angle between $\mathbf{a}$ and $\mathbf{e}_3(\phi)$ (see Figure 1.1), $z'(s) = \cos\theta(s)$ and $r'(s) = \sin\theta(s)$. The inward pointing normal is

$$\mathbf{b}(s,\phi) = \mathbf{a} \times \mathbf{e}_2(\phi) = -\cos\theta\mathbf{e}_1(\phi) + \sin\theta\mathbf{e}_3(\phi). \tag{1.4}$$

Let $s_0 \in (0,\ell_d)$, and let the vector $\mathbf{n}_1(s_0,\phi)$ denote the resultant stress defined at each point of the curve $\phi \to \mathbf{x}(s_0,\phi)$. Then $\mathbf{n}_1(s_0,\phi)$ represents the density of the resultant contact force generated by the part of S with $s \geq s_0$ acting on the portion of S with $s < s_0$. Similarly, let $0 \leq \phi_0 < 2\pi$ and let $\mathbf{n}_2(s,\phi_0)$ denote the resultant stress defined at each point of the curve $s \to \mathbf{x}(s,\phi_0)$. The vector $\mathbf{n}_2(s,\phi_0)$ represents the density of resultant contact force generated by the part of S with $\phi_0 \leq \phi < \phi_0 + \varepsilon$ acting on the part of S with $\phi_0 - \varepsilon < \phi < \phi_0$. We choose $\varepsilon > 0$ small enough that $0 \leq \phi_0 - \varepsilon$ and $\phi_0 + \varepsilon \leq 2\pi$. Both $\mathbf{n}_1$ and $\mathbf{n}_2$ are measured per unit length in the deformed configuration.

Because the balloon is modeled as a membrane, we can ignore all bending moments and couples. Furthermore, under the assumption of axisymmetry, we can write the contact forces as

$$\begin{aligned} \mathbf{n}_1(s,\phi) &= \sigma_m(s)\mathbf{a}(s,\phi), \\ \mathbf{n}_2(s,\phi) &= \sigma_c(s)\mathbf{e}_2(\phi), \end{aligned}$$

where σ_m is the meridional stress and σ_c the circumferential stress. Next, we consider the equilibrium of a test patch A, where

$$A = \{\mathbf{x}(\xi,\psi) \mid s_0 \leq \xi \leq s,\ 0 \leq \psi \leq \phi\},$$

for some $s_0 \in (0,\ell_d)$ and $\phi \in (0,2\pi)$. The forces acting on A are the internal forces, $\mathbf{n}_1(s,\phi)$ and $\mathbf{n}_2(s,\phi)$, and the external forces,

$$\mathbf{f}(s,\phi) = -p(s)\mathbf{b}(s,\phi) - w(s)\mathbf{e}_3(\phi) - f_D(s)\mathbf{e}_3(\phi), \tag{1.5}$$

where p is hydrostatic pressure due to the difference between the densities of the lifting gas and the ambient air, w is balloon film weight, and f_D is the aerodynamic pressure density due to drag. All external forces are measured per unit area in the deformed configuration.

In general, the drag on a submersed body exerted by a fluid that is in motion through the fluid is

$$\mathbf{F}_D = -\tfrac{1}{2}\rho_{air} C_D A_D |\mathbf{v}_B - \mathbf{v}_{air}|(\mathbf{v}_B - \mathbf{v}_{air}), \tag{1.6}$$

where C_D is the drag coefficient, ρ_{air} is the density of the air, A_D is the area of the projection of the body on the plane perpendicular to the direction of motion, $\mathbf{v}_B$ is the velocity of the balloon, $\mathbf{v}_{air}$ is the velocity of the atmosphere (see [7, p. II-13] and [10, Sec. 4.3]). In our applications, the velocity of the balloon will be in the $\pm\mathbf{k}$ directions. We specify the magnitude of the velocity of the balloon $|\mathbf{v}_B| = v_B$ and assume that $|\mathbf{v}_{air}| = 0$. For a descending balloon, $\mathbf{F}_D$ is given by

$$\mathbf{F}_D = -\tfrac{1}{2}\rho_{air} C_D A_D v_B^2 \mathbf{k}. \tag{1.7}$$

We define $f_D(s) = \mathbf{F}_D \cdot \mathbf{e}_3(\phi)$, and it follows from Eq. (1.7) that the aerodynamic pressure density is

$$f_D(s) = -\tfrac{1}{2}\rho_{air} C_D v_B^2 A_D. \tag{1.8}$$

From Eq. (1.8), we see that $f_D(s)$ can be expressed as

$$f_D(s) = -\tfrac{1}{2}\rho_{air} C_D v_B^2 \mathbf{I}_{[-\pi/2,0]}(\theta(s)) \sin\theta(s), \tag{1.9}$$

where $\mathbf{I}$ is the indicator function, i.e.,

$$\mathbf{I}_{[a,b]}(x) = \begin{cases} 1, & x \in [a,b] \\ 0, & x \notin [a,b] \end{cases}.$$

We will write $f_D(\theta)$ to emphasize the dependence of f_D on $\theta = \theta(s)$. The parameter C_D depends on a variety of factors (see [7, p. II-13]); for a descending balloon, we will assume $C_D = 0.8$. For an ascending balloon, f_D is similarly defined with $C_D = 0.4$ and indicator function $\mathbf{I}_{[0,\pi/2]}$. Note, for an ascending balloon $f_D \geq 0$, while for a descending balloon $f_D \leq 0$. The caps will be modeled as an added thickness, so w depends on s.

The total force acting on A is

$$\begin{aligned} 0 \;=\; & \int_0^{\phi} \sigma_m(s)\mathbf{a}(s,\psi) r(s) d\psi - \int_0^{\phi} \sigma_m(s_0)\mathbf{a}(s_0,\psi) r(s_0) d\psi \\ & + \int_{s_0}^{s} \sigma_c(\xi)\mathbf{e}_2(\phi) d\xi - \int_{s_0}^{s} \sigma_c(\xi)\hat{\mathbf{e}}_2(0) d\xi + \int_{s_0}^{s}\int_0^{\phi} \mathbf{f}(\xi,\psi) r(\xi) d\psi d\xi. \end{aligned} \tag{1.10}$$

Differentiating Eq. (1.10) with respect to s and ϕ and using $\partial\hat{\mathbf{e}}_2/\partial\phi = -\hat{\mathbf{e}}_1$, we are lead to the following equilibrium equations,

$$\frac{\partial}{\partial s}(r\sigma_m\mathbf{a}) - \sigma_c\mathbf{e}_1(\phi) + r\mathbf{f} = \mathbf{0}. \tag{1.11}$$

In this report, when discussing a descending (or ascending balloon), we ignore the dynamics of the balloon flight and assume that the balloon is in a quasi-static equilibrium state as given by Eq. (1.11).

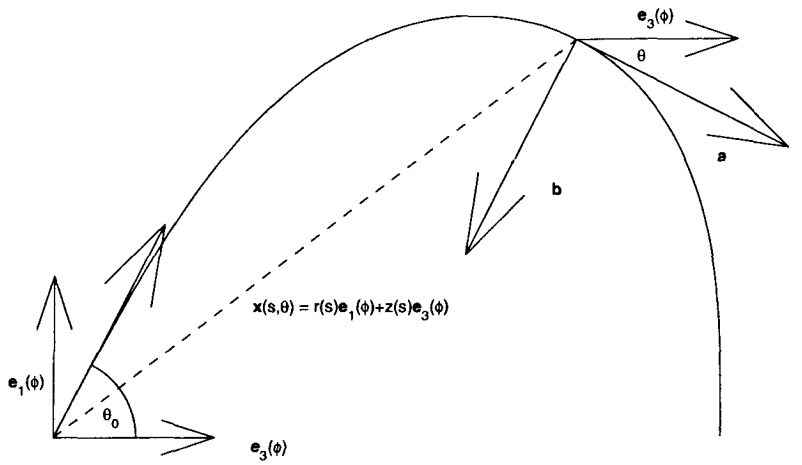

Figure 1.1: Generating curve for a natural-shape balloon (at float)

1.1.3 The natural-shape model equations

In this section, we formulate the natural-shape model, including boundary conditions for float and descent shapes (ascending shapes can be considered with some slight modifications). Projecting Eqs. (1.11) onto the $\mathbf{e}_3(\phi)$ and $\mathbf{e}_1(\phi)$ directions, we obtain,

$$0 = \frac{d}{ds}(r\sigma_m\cos\theta) - rw - pr\sin\theta - rf_D(\theta), \tag{1.12}$$

$$0 = \frac{d}{ds}(r\sigma_m\sin\theta) - \sigma_c + pr\cos\theta, \tag{1.13}$$

respectively. After carrying out the differentiation and rearranging terms in (1.12)–(1.13), we obtain

$$0 = \frac{d}{ds}(r\sigma_m)\cos\theta - (r\sigma_m)\sin\theta\frac{d\theta}{ds} - rw - pr\sin\theta - rf_D(\theta), \tag{1.14}$$

$$0 = \frac{d}{ds}(r\sigma_m)\sin\theta + (r\sigma_m)\cos\theta\frac{d\theta}{ds} - \sigma_c + pr\cos\theta.$$

If we substitute $p = b(z+z_0)$, where z_0 is the distance from the zero-pressure level to the bottom of the balloon and b is the specific buoyancy of the lifting gas, and solve for $d\theta/ds$ and $d(r\sigma_m)/ds$, we obtain

$$(r\sigma_m)\frac{d\theta}{ds} = \sigma_c\cos\theta - rw\sin\theta - br(z+z_0) - rf_D(\theta)\sin\theta, \tag{1.15}$$

$$\frac{d}{ds}(r\sigma_m) = \sigma_c\sin\theta + rw\cos\theta + rf_D(\theta)\cos\theta. \tag{1.16}$$

While b is assumed to be known as a function of altitude, the value of b depends on a number of parameters (e.g., $b = b(T_a, T_b, \rho_a, \rho_g)$ where T_a is temperature of the air, T_g is the temperature of

the gas, ρ_a is the the density of the air, and ρ_g is the density of the gas). See Appendices A-B for further details on the calculation of b. The zero-pressure level z_0 is determined during the solution process. Normally , we assume $z_0 = 0$ and $v_B = 0$ at float. However, if $v_B \neq 0$, we can also compute a natural shape.

Since the generating curve is parametrized by arc-length, we see that

$$\frac{dz}{ds} = \cos\theta \text{ and } \frac{dr}{ds} = \sin\theta. \tag{1.17}$$

It will be convenient to define the total film load T in the meridional direction, i.e.,

$$T = 2\pi r\sigma_m. \tag{1.18}$$

Multiplying both Eqs. (1.15)-(1.16) by 2π, substituting T for $2\pi r\sigma_m$, and setting $\sigma_c = 0$ (an assumption of the natural shape), we have

$$\frac{d\theta}{ds} = -2\pi r\left(w\sin\theta + b(z+a) + f_D(\theta)\sin\theta\right)/T, \tag{1.19}$$

$$\frac{dT}{ds} = 2\pi r\left(w + f_D(\theta)\right)\cos\theta. \tag{1.20}$$

For applications considered here, we will assume that a load L is suspended from the base of the balloon. Thus,

$$T(0) = L/\cos\theta_0, \tag{1.21}$$

where $\theta(0) = \theta_0$ and θ_0 is one-half the "cone-angle" at the base of the balloon (see Figure 1.1). Note, θ_0 is not known apriori and must be computed based on certain parameter values and boundary conditions. If there is no load at the top of the balloon, then $\theta = -\pi/2$ at the top.

1.1.4 Problem formulation using the parallel shooting method

Standard Model

The governing differential equations for a natural-shape balloon in terms of T are

$$\frac{d\theta}{ds} = -2\pi r(w\sin\theta + b(z+z_0) + rf_D(\theta)\sin\theta)/T, \tag{1.22}$$

$$\frac{dT}{ds} = 2\pi r(w + f_D(\theta))\cos\theta, \tag{1.23}$$

$$\frac{dz}{ds} = \cos\theta, \tag{1.24}$$

$$\frac{dr}{ds} = \sin\theta. \tag{1.25}$$

At the top of the balloon, we assume

$$\begin{aligned} \theta(\ell) &= -\tfrac{1}{2}\pi, \\ r(\ell) &= 0. \end{aligned} \tag{1.26}$$

The initial conditions for Eqs. (1.22)-(1.25) are

$$\begin{aligned} \theta(0) &= \theta_0, \\ T(0) &= L/\cos\theta_0, \\ z(0) &= 0, \\ r(0) &= 0. \end{aligned} \tag{1.27}$$

For a given pair (θ_0, ℓ) and weight density $w(s)$, Eqs. (1.22)–(1.25) can be integrated over the interval $0 < s < \ell$ beginning with the initial conditions in Eqs. (1.27). Using a shooting method, one determines $(\theta_0, \ell) = (\theta_{0,d}, \ell_d)$ and the functions $\theta(s;\theta_{0,d},\ell_d)$, $T(s;\theta_{0,d},\ell_d)$, $z(s;\theta_{0,d},\ell_d)$, and $r(s;\theta_{0,d},\ell_d)$ that satisfy Eq. (1.22)–(1.25), and Eqs. (1.26), i.e.,

$$\begin{aligned} \theta(\ell_d;\theta_{0,d},\ell_d) &= -\tfrac{1}{2}\pi, \\ r(\ell_d;\theta_{0,d},\ell_d) &= 0. \end{aligned} \tag{1.28}$$

Such a solution automatically satisfies Archimedes principle. For if we multiply Eq. (1.14) by 2π, integrate from $s = 0$ to $s = \ell_d$, and used the identity,

$$r(z+z_0)\frac{dr}{ds} = \tfrac{1}{2}\frac{d}{ds}\left(r^2(z+z_0)\right) - \tfrac{1}{2}r^2\frac{dz}{ds},$$

we obtain

$$-T(\theta_{0,d})\cos(\theta_{0,d}) = 2\pi\int_0^{\ell_d} wrds - bV - F_D, \tag{1.29}$$

and after rearränging terms,

$$L + W_B = bV + F_D, \tag{1.30}$$

where W_B is the total weight of the balloon system (shell, caps, and load tapes) and F_D is the total drag.

In the natural-shape model in [3], the weights of the caps and load tapes were added to the payload. In the model presented here, the balloon system includes two caps that are modeled as an added thickness. We will assume that the number of gores in a complete shape is n_g. The weight of the load tapes will be incorporated by modifying w appropriately. The lengths of the generators for the caps are denoted by c_1, c_2, respectively and are assumed to be known. For a given ℓ, let $s_1 = \ell - c_1$ and $s_2 = \ell - c_2$ denote the location of caps' edges. This means that $w(s_i+0) \neq w(s_i-0)$ for $i = 1,2$ and $d\theta/ds$ and dT/ds are discontinuous (another discontinuity arises when $f_D \neq 0$).

Next, we outline a parallel shooting method for computing a design shape with a variable thickness. See [13] and [14] for a discussion of the parallel shooting method. In the following, we

denote the length of the first, second, and third interval by $l_1 = s_1$, $l_2 = s_2 - s_1$, and $l_3 = \ell - s_2$, respectively. We divide $n_g w_t$ by $2\pi r(s)$ in order to get the average weight density of tape with respect to area. The total length ℓ is not known beforehand and will be computed as part of the solution process. We define $w(s)$ as follows,

$$w(s) = w_{film}(s) + n_g w_t/(2\pi r(s)), \quad 0 < s < \ell,$$

where

$$w_{film}(s) = \begin{cases} w_f, & 0 \le s \le l_1 \\ 2w_f, & l_1 < s \le l_2 \\ 3w_f, & l_2 < s \le \ell \end{cases}, \tag{1.31}$$

w_f is the weight density of a single layer of balloon film, w_t is the load tape weight density and n_g is the number of gores. Eq. (1.31) can be easily modified to accommodate balloons with varying material properties, other than the thickness due to the caps. Eqs. (1.22)–(1.25) are equivalent to

$$\frac{d\theta_i}{ds} = -2\pi r_i \left(w_i \sin\theta_i + b(z_i + z_0) + f_D(\theta_i)\sin\theta_i\right)/T_i, \tag{1.32}$$

$$\frac{dT_i}{ds} = 2\pi r_i \left(w_i + f_D(\theta_i)\right)\cos\theta_i, \tag{1.33}$$

$$\frac{dz_i}{ds} = \cos\theta_i, \tag{1.34}$$

$$\frac{dr_i}{ds} = \sin\theta_i, \tag{1.35}$$

for $s_{i-1} < s < s_i$ and $i = 1,2,3$, with the convention that $s_0 = 0$ and $s_3 = \ell$. For a function such as $w(s)$, we will follow the convention that $w_i(s) = w(s)$ for $s_{i-1} < s < s_i$, and similar definitions for the other relevant functions θ_i, T_i, z_i, r_i. Eqs. (1.32)–(1.35) are supplemented by the initial conditions,

$$\begin{aligned} \theta_1(0) &= \theta_1^0, \\ T_1(0) &= L/\cos\theta_1^0, \\ r_1(0) &= 0, \\ z_1(0) &= 0, \\ \theta_i(s_i) &= \theta_{i+1}^0, \quad i = 1,2, \\ T_i(s_i) &= T_{i+1}^0, \quad i = 1,2, \\ z_i(s_i) &= z_{i+1}^0, \quad i = 1,2, \\ r_i(s_i) &= r_{i+1}^0, \quad i = 1,2. \end{aligned} \tag{1.36}$$

Eqs. (1.36) involve nine explicit free parameters $\{\theta_1^0, \theta_2^0, T_1^0, T_2^0, z_1^0, z_2^0, r_1^0, r_2^0\}$ and the implicit parameter ℓ. Using the conditions at the top of the balloon given by Eq. (1.28), we are led to ten auxiliary conditions involving the unknown parameters,

$$\begin{aligned}
\theta_i(s_i) &= \theta_{i+1}^0, \quad i = 1,2, \\
T_i(s_i) &= T_{i+1}^0, \quad i = 1,2, \\
r_i(s_i) &= r_{i+1}^0, \quad i = 1,2, \\
z_i(s_i) &= z_{i+1}^0, \quad i = 1,2, \\
r_3(\ell) &= 0, \\
\theta_3(\ell) &= -\tfrac{1}{2}\pi.
\end{aligned} \tag{1.37}$$

By construction, the functions $\theta(s) = \theta_i(s)$, $T(s) = T_i(s)$, $r(s) = r_i(s)$, and $z(s) = z_i(s)$ for $i = 1,2,3$ are continuous on $0 < s < \ell_d$.

Following the approach of [13], a new independent variable $\hat{s}$ is introduced on each interval by the transformation

$$\hat{s} = (s - \tau_i)/l_i, \quad i = 1,2,3,$$

where $\tau_1 = 0, \tau_2 = l_1$ and $\tau_3 = l_1 + l_2$. By construction, $0 < \hat{s} < 1$ on each subinterval. Let $\hat{z}_i = z_i(\hat{s}), \hat{r}_i = r_i(\hat{s}) \ldots$, and so on. In the rescaled coordinates, we find Eqs. (1.32)–(1.35) can be written as

$$\frac{d\hat{\theta}_i}{d\hat{s}} = -2\pi\hat{r}_i l_i \left(w_i \sin\hat{\theta}_i + b(\hat{z}_i + z_0) + f_D(\hat{\theta}_i)\sin\hat{\theta}_i\right)/\hat{T}_i, \tag{1.38}$$

$$\frac{d\hat{T}_i}{d\hat{s}} = 2\pi\hat{r}_i l_i \left(w_i + f_D(\hat{\theta}_i)\right)\cos\hat{\theta}_i, \tag{1.39}$$

$$\frac{d\hat{z}_i}{d\hat{s}} = l_i \cos\hat{\theta}_i, \tag{1.40}$$

$$\frac{d\hat{r}_i}{d\hat{s}} = l_i \sin\hat{\theta}_i, \tag{1.41}$$

for $i = 1,2,3$.

The auxiliary conditions in the rescaled coordinates are

$$\begin{aligned}
\hat{\theta}_i(1) &= \hat{\theta}^0_{i+1}, \quad i=1,2,\\
\hat{T}_i(1) &= \hat{T}^0_{i+1}, \quad i=1,2,\\
\hat{r}_i(1) &= \hat{r}^0_{i+1}, \quad i=1,2,\\
\hat{z}_i(1) &= \hat{z}^0_{i+1}, \quad i=1,2,\\
\hat{r}_3(1) &= 0,\\
\hat{\theta}_3(\ell) &= -\tfrac{1}{2}\pi.
\end{aligned} \tag{1.42}$$

The problem of computing a standard natural-shape balloon is to find a solution of Eqs. (1.38)-(1.41) on the interval $0 < \hat{s} < 1$ satisfying Eqs. (1.42) with $v_B = 0$ and $z_0 = 0$.

Natural shape design with drag

Eqn. (1.30) suggests there is a one-parameter family of design shapes, parametrized by v_B. We make the standard assumptions that $\sigma_c = 0$ and $z_0 = 0$, but do not assume that v_B is zero. The net effect is that the volume of the design shape is reduced and the balloon is taller and narrower for decreasing v_B. Natural shape balloons with drag will be computed in Section 1.5.2. A *natural shape design with drag* is a solution of Eqs. (1.38)-(1.41) on the interval $0 < \hat{s} < 1$ satisfying Eqs. (1.42) with $v_B \neq 0$ and $z_0 = 0$.

1.1.5 Partially inflated natural shape balloons

In the following, we assume that the design shape is known and the generating curve for the design shape is

$$(R_d(s), Z_d(s)), \quad 0 < s < \ell_d.$$

If $v_B = 0$, in our exposition, we assume that

$$bV = b_d V_d \tag{1.43}$$

where V_d is the design volume, b_d is the buoyancy at float, and V is the current volume. Eq. (1.43) implies that $b = b_d V_d / V$. Since $V < V_d$, the balloon envelope is not fully deployed. If $v_B \neq 0$, we assume $b = \tau b_k$, and Archimedes Principle and Eq. (1.30) imply that the volume must satisfy $V = (W_B + L - F_D)/b$.

To account for excess material, we modify the film weight density (replacing $w(s) \to w(s)R_d(s)/r(s)$). In particular, Eqs. (1.22)-(1.25) are replaced by (see [3])

$$\begin{aligned}
\frac{d\theta}{ds} &= -2\pi(R_d(s)w\sin\theta + br(z+z_0) + rf_D(\theta)r\sin\theta)/T, && (1.44)\\
\frac{dT}{ds} &= 2\pi(R_d(s)w + rf_D(\theta))\cos\theta, && (1.45)\\
\frac{dz}{ds} &= \cos\theta, && (1.46)\\
\frac{dr}{ds} &= \sin\theta. && (1.47)
\end{aligned}$$

Since we assume that the generating curve is inextensible, ℓ_d is constant, and we introduce the zero-pressure level z_0 as the parameter to be determined. In particular, we replace Eqs. (1.26), by

$$\begin{aligned}
\theta(\ell_d;\theta_1^0,z_0) &= -\tfrac{1}{2}\pi,\\
r(\ell_d;\theta_1^0,z_0) &= 0.
\end{aligned} \qquad (1.48)$$

When the volume of the balloon gets very small, θ_1^0 is nearly zero, and it virtually impossible to solve Eqs. (1.48) with an ordinary shooting method. This problem was circumvented in [3], by subdividing $0 < s < \ell_d$ and solving the governing equations with a parallel shooting method. For the present application, we subdivide the three intervals $[0,l_1]$, $[l_1,l_2]$, $[l_2,\ell_d]$. For a given subdivision obtained by adding adding new break point s_k, four additional parameters $\{\theta_k^0, T_k^0, r_k^0, z_k^0\}$ are introduced with four additional auxiliary equations,

$$\begin{aligned}
\theta_{k-1}^0(s_k) &= \theta_k^0,\\
T_{k-1}^0(s_k) &= T_k^0,\\
r_{k-1}^0(s_k) &= r_k^0,\\
z_{k-1}^0(s_k) &= z_k^0.
\end{aligned} \qquad (1.49)$$

After relabeling of quantities, for n subdivisions there will be a total of $2+4(n-1)$ parameters to be determined, i.e.,

$$z_0, \theta_1^0, \theta_2^0, T_2^0, r_2^0, z_2^0, \ldots, \theta_{n-1}^0, T_{n-1}^0, r_{n-1}^0, z_{n-1}^0.$$

The auxiliary equations are rescaled in the same manner as Eqs. (1.38)-(1.41).

1.1.6 Numerical results

Standard design shape

In the following, we present results on descending axisymmetric inextensible natural shape balloons using the parallel shooting method described in Section 1.4. We consider a design shape based on the parameters in Table 1.1. The values in Table 1.1 correspond roughly to a solar Montgolfiere balloon made of 3.5 micron mylar with a payload of 6 kg. The examples were chosen to illustrate how the shapes varies as certain parameters change. We first compute a design shape with $v_B = 0$. The height and diameter of the design shape is shown in Table 1.1. We then compute shapes for $\tau = 2$ and $\tau = 5$. When $v_B = 0$ and $\tau = 2$, we find $V = 0.5\,V_d$. When $v_B = 0$ and $\tau = 5$, we find $V = 0.2\,V_d$. In Figures 1.2- 1.3, the design shape profile is shown to the left of the partially inflated ascent shape. Plots of $\theta(s), T(s), r(s), z(s)$ are also shown.

In Figure 1.2(a), we present an ascent shape with $V = 0.5\,V_d$. To eliminate drag from our model, we set $C_D = 0$. The variation in shading indicate the subintervals used in the parallel shooting method (8 subintervals were used). Next, we set $C_D = 0.8$ and computed a corresponding solution shown in Figure 1.2(b). Because of Archimedes Principal (see Eq. (1.30)), if we maintain the same b and increase F_D, then the effective volume V must decrease. In the zero drag case, the total meridional tension increases monotonically. With drag acting on the lower portion of the balloon, the tension is reduced. Next, we increased the velocity and air density and considered shapes with a smaller volume. In Figure 1.3(a), we present an ascent shape with $V = 0.2\,V_d$. Next, we set $C_D = 0.8$ and computed a corresponding solution (see Figure 1.3(b)). In Table 1.2, we compare quantities related to the shapes presented in Figure 1.2 and Figure 1.3.

Remark. It should be noted that the assumption, $b\,V = b_d\,V_d$ is more relevant to ascent shapes than for a descending balloon that is being inflated. For a descending balloon that is being inflated (such as a Solar Montgolfiere), the higher buoyancy values occur when the balloon is near full inflation and the low values occur for low volumes. Nevertheless, the results presented in this section are for demonstration purposes and illustrate how such shapes can be analyzed.

Natural shape with drag

In this section, we consider a balloon descending with a constant velocity and compute the corresponding design shape. We assume a balloon with a 6 kg payload and a balloon envelope with density 8 kg/m^2. Additional design parameters are presented in Table 1.3.

In Figure 1.4, we present a family of design shapes parametrized by v_B. In Figure 1.4(a), $v_B = 0$. In Figures 1.4(b)-(d), we present design shapes with velocities -2 m/sec, -4 m/sec, and -6

Table 1.1: Design Parameters for Test Case

Parameter	Description	Design Value
b_d	Buoyancy	3.9020375e-04 lbf/ft^3
L	Payload	13.22750 lbf
w_f	Film weight density	1.43369e-03 lbf/ft^2
w_t	Tape weight density	0 lbf/ft
n_g	Number of gores	27
V_d	Volume	62290 ft^3
ℓ_d	Gore length	76.738 ft
θ_0	Angle at base	59.32 deg
$\max Z_d$	Balloon Height	45.76 ft
$2 \cdot \max R_d$	Diameter	53.219 ft
A_T	Surface Area	7727.26 ft^2
W_T	Gross Weight	24.306 lbf

Table 1.2: Comparison of descending shapes with and without drag

Quantity	Description	$0.5\,V_d$		$0.2\,V_d$	
C_D	Drag coefficient	0	0.8	0	0.8
v_B (ft/sec)	Velocity of balloon	0	-4.59	0	-16.40
F_D (lbf)	Total drag	0	7.06	0	21.91
z_0 (ft)	Zero-pressure level	29.97	34.47	42.48	57.37
b (lbf/ft^3)	Buoyancy	$2b_d$	$2b_d$	$5b_d$	$5b_d$
$\max r$ (ft)	Max radius	19.86	17.60	14.40	6.64
$\max z$ (ft)	Height	58.11	60.74	63.69	71.99

(a) Without drag

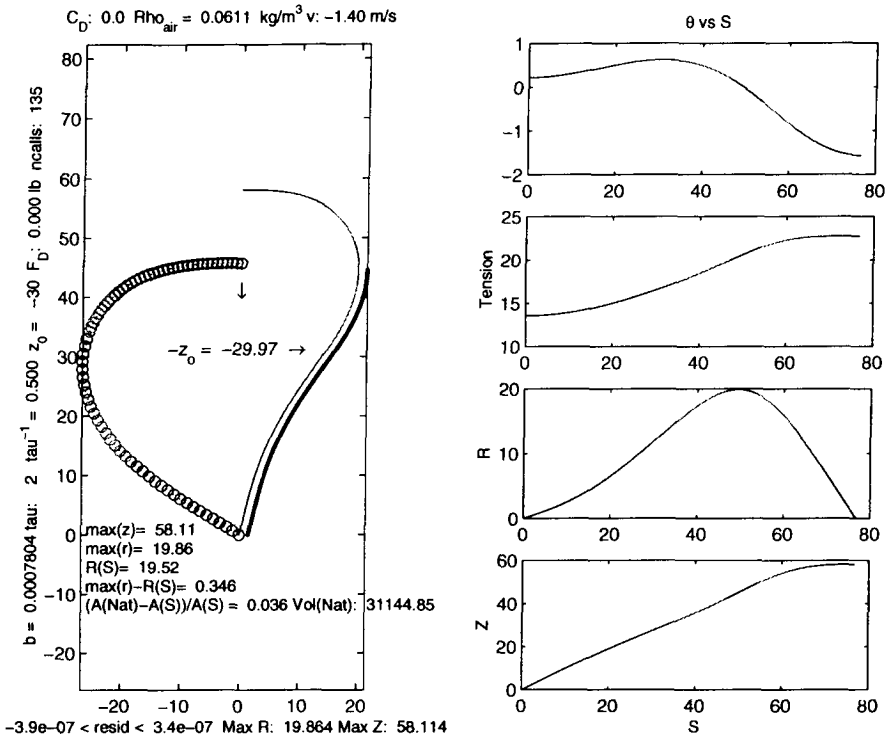

(b) With drag

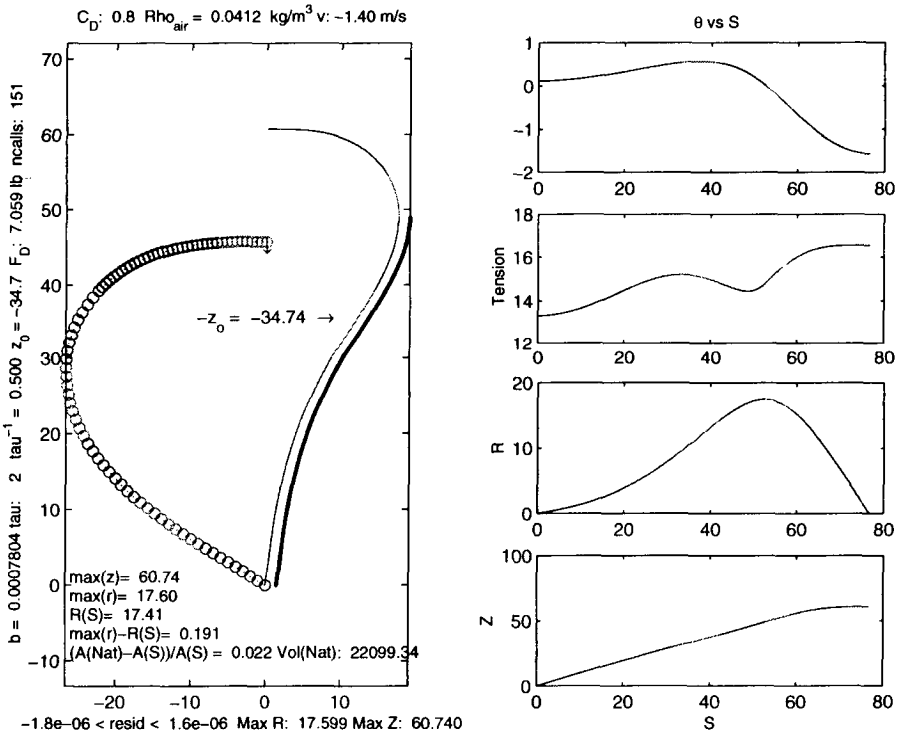

Figure 1.2: Comparison of descent shapes with and without drag

(a) Without drag

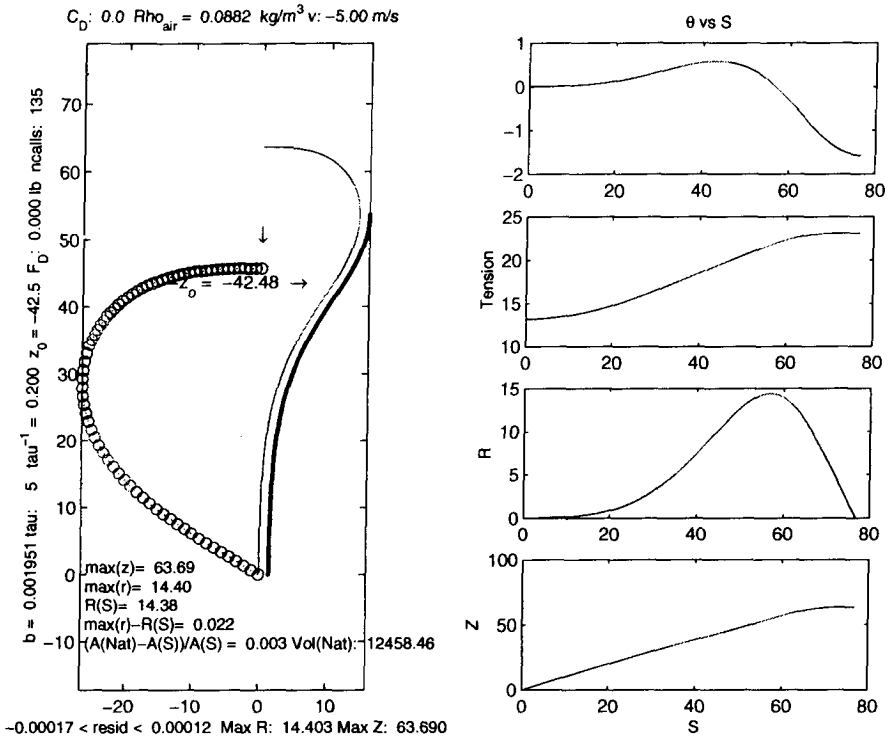

(b) With drag

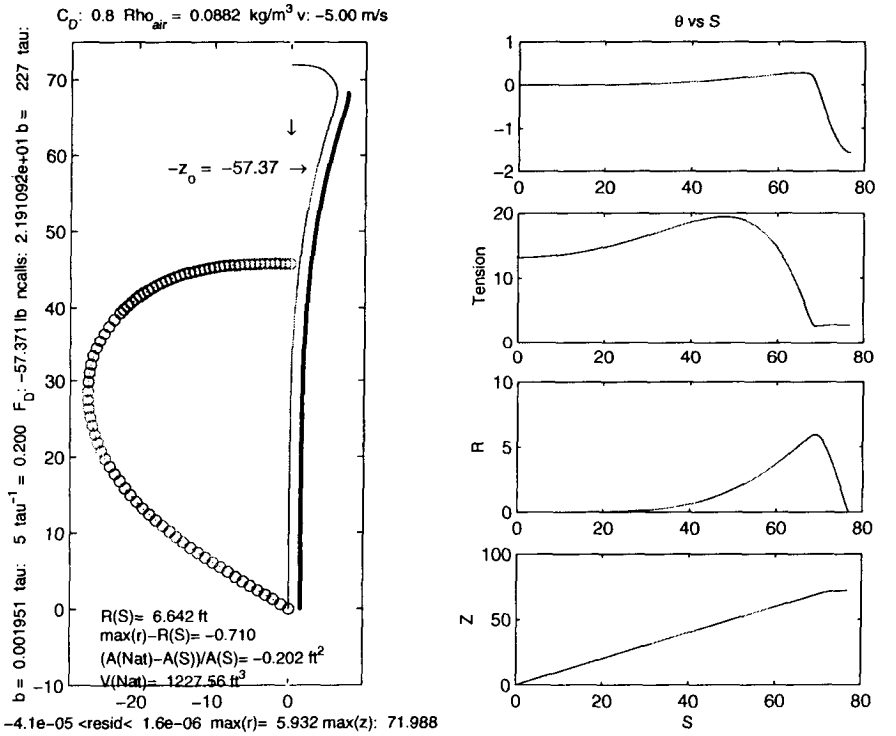

Figure 1.3: Comparison of descent shapes with and without drag at low volume

Table 1.3: Parameter values for a natural shape design with drag

Quantity	Value
Payload	6 kg
Film density	8 g/m^2
ρ_{air}	0.00827 kg/m^3
ρ_{gas}	0.00541 kg/m^3
b	280.764 kN/m^3

Table 1.4: Comparison of natural shapes with drag as a function of velocity

Velocity (m/sec)	0	-2	-4	-10
Gore length (m)	36.87	30.08	33.86	23.68
θ_0 (deg.)	68.06	67.03	63.84	43.60
Height (m)	20.42	20.06	19.07	14.88
Diameter (m)	26.63	26.05	24.38	16.12
Volume (m^3)	7291.98	6811.29	5555.57	1619.63
Surface Area (m^2)	1856.87	1774.93	1551.50	689.73
Mass (kg, $M_B + M_{Load}$)	20.85	20.20	18.41	11.52

m/sec. As the velocity increases in magnitude, the volume of the design shape is reduced and the ratio of diameter to height is also reduced. Once a design shape has been computed, we can also determine partially inflated natural shapes as we did in the previous section.

In Table 1.4. we present computed quantities related to the family of design shapes.

1.1.7 Remarks on natural-shape analysis

It is interesting to compare the results from Table 1.4 with that of a sphere of comparable volume. For example, consider the case when $v_B = -10$ m/sec. In this case, the volume, diameter, and balloon weight of the natural shape is 1619 m^3, 16.12 m, and 5.517 kg. For a sphere of the same volume, the diameter is 14.56 m and its weight is 5.334 kg. Even thought the natural shape weighs only 0.18 kg more than the sphere, it produces a drag equivalent to 6.89 kg, versus 5.623 kg for the sphere. The natural shape produces over 22% more drag than a sphere with the same volume.

Aerodynamic drag can be incorporated into a model for inextensible partially inflated natural shape balloons. While real balloons are not inextensible and the hoop stresses are not zero, the results in this section can be applied to elastic balloons that are not axisysmmetric. In Section 2, we show how to extend this approach to our EM-model for a more general class of balloon shapes.

Figure 1.4: Design shapes with drag (a) $v_B = 0$ m/sec; (b) $v_B = -2$ m/sec; (c) $v_B = -4$ m/sec; (d) $v_B = -10$ m/sec.

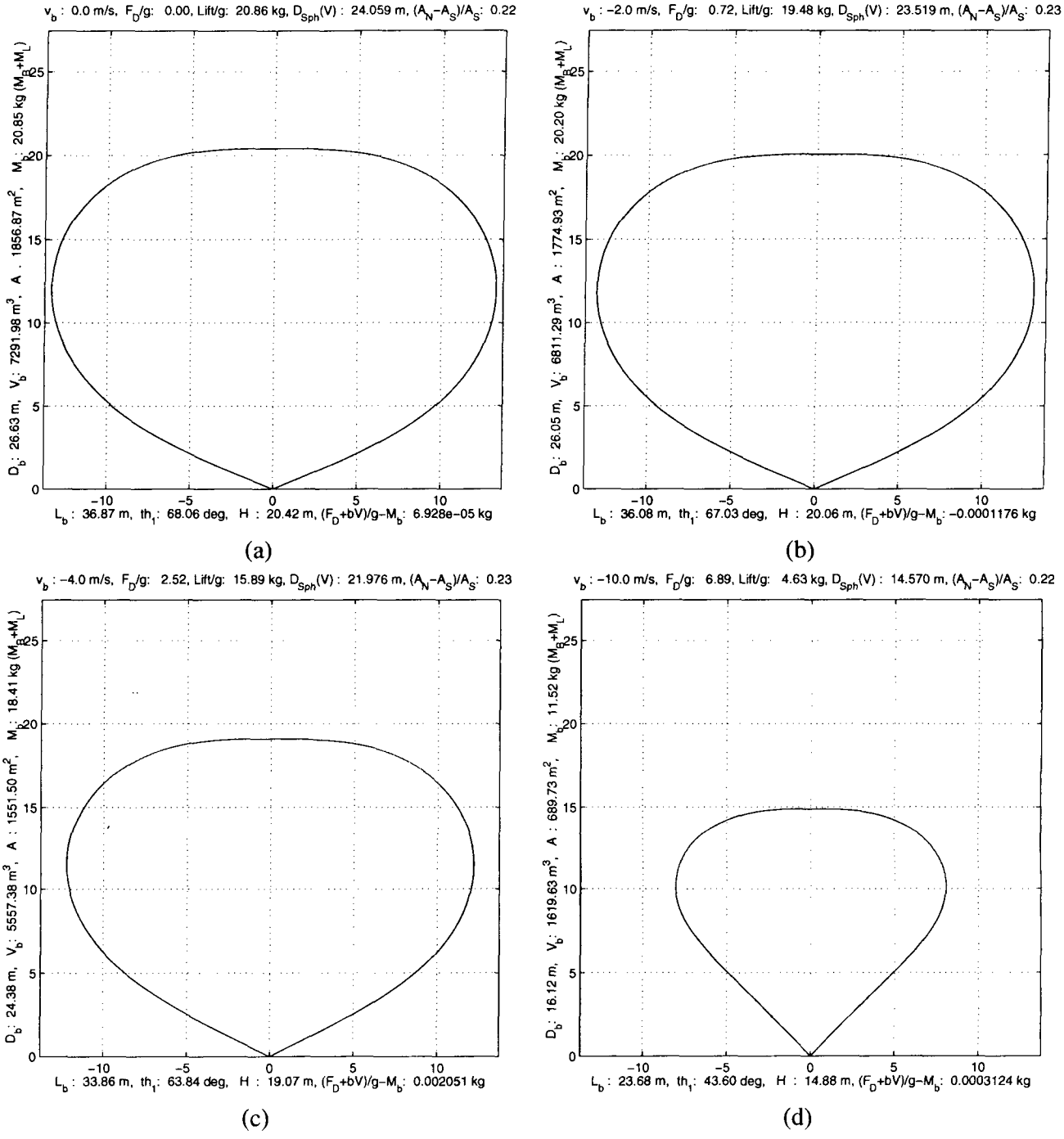

1.2 Aerodynamic loading of partially inflated balloons with lobes

In this section, we outline a mathematical model for the aerodynamic loading of a lobed balloon shape. For simplicity and ease of exposition, we focus primarily on the case of drag on a descending balloon. We adapt the method of Chapter 1 to balloon shapes with and without lobes. Our approach is to derive an expression for the potential energy due to drag, so it can be added to our model for lobed energy minimizing shapes (i.e., LEM-shapes).

1.2.1 Background

A feature characterizing partially inflated scientific balloons is a lobe structure surrounding the gas bubble. When the gas bubble is of insufficient volume, the balloon envelope will collapse, forming folds of excess material and lobes. We present a mathematical model for a balloon shape with such features that is subjected to aerodynamic loading. We formulate a variational principal for the balloon system, and seek to determine a shape that minimizes energy subject to a volume constraint. The energy includes film and load tape strain, film and load tape weight, hydrostatic pressure, and drag.

Based on observations of real balloons, it is reasonable to assume that lobed structures are periodic. Balloon shapes with lobes were investigated in [5] using variational techniques where the energy of the balloon system included hydrostatic pressure and film weight. The energy of the balloon system was minimized subject to constraints on the volume and the lengths of certain fibers. Geometrically, the shapes in [5] possessed many features seen in real balloons: lobes surrounding the gas bubble, a sphere-like top, internal folds of excess balloon fabric, and flat wing-like structures (fins) hanging beneath the gas bubble. However, the formulation of the problem did not include strain energy. In [2] and [4], the film and load tape strain energies were considered for shapes modeled by a half-gore. In this work, we formulate a variational principal for a partially inflated balloon subject to aerodynamic drag in such a way that a lobed structure can (but not necessarily) form. While drag influences the balloon shape, lobes will form independently of drag.

In the following, let $S(V,q,r)$ denotes a deformed balloon with volume V, q lobes, and r gores per lobe. The total number of gores is n_g and $n_g = rq$. If it is clear from context, we will omit certain arguments and write S instead of $S(V,q,r)$. S_F denotes a fundamental section of S (S_F is centered about a vertical plane of reflectional symmetry). By symmetry arguments, r is odd, i.e., $r = 2k+1$. A superscript $j = 1,2,\ldots,r$ denotes a quantity related to the jth gore of S_F. When $r = 1$, the balloon shape can be modeled by a half-gore. When $r > 1$, the balloon can have lobes. Viewed from above, the discrete design shape will have the symmetries of a regular polygon with

n_g sides. In general, $S(V,q,r)$ will be invariant under the dihedral group D_q and viewed from above, it will have the symmetries of a regular polygon with q sides. To simplify our exposition, we will consider a natural-shape design with $n_g = 27$ (note, $C_{27} \subset C_9 \subset S_3$). A shape with D_9 symmetry has nine lobes and each complete lobe is constructed from 3 gores.

1.2.2 Potential energy for aerodynamic drag

Aerodynamic drag can be introduced into our balloon shape model by adapting Eq. (1.6) appropriately. Consider an arbitrary facet in the triangulation of a balloon shape that is not part of a fold. Let v_0, v_1, v_2 denote the vertices, and $\vec{e}_0 = v_1 - v_0$, $\vec{e}_1 = v_2 - v_1$, $\vec{e}_2 = v_0 - v_2$. We assume that v_0, v_1, v_2 are ordered in such a way that the unit normal $\mathbf{n} = \vec{e}_0 \times \vec{e}_1 / |\vec{e}_0 \times \vec{e}_1|$ points outward. For a balloon descending with a velocity $\mathbf{v}_B = -v_B\mathbf{k}$, the drag on typical triangle T is:

$$F_D(T) = \begin{cases} -\frac{1}{2}\rho_{air} C_D v_B^2 \, \vec{dA} \cdot \mathbf{k}, & 0 < \arccos(-\mathbf{k}\cdot\mathbf{n}) < \pi/2, \\ 0 & \text{otherwise}, \end{cases} \tag{1.50}$$

where $\vec{dA} = \frac{1}{2}|e_0 \times e_1|\mathbf{n}$. Adding up the drag contributions of each facet that contacts the atmosphere yields the total potential energy of the drag on the balloon, i.e.,

$$E_D(S) = -\tfrac{1}{2}\int_S \rho_{air} C_D v_B^2 \, \vec{dA} \cdot \mathbf{k}. \tag{1.51}$$

1.2.3 Mathematical model for aerodynamically loaded balloon shapes

In Table 1.5, we present design parameters that are used for the illustrations in this section. In the following, the reader should refer to Figure 1.5 for notation related to the reference configuration. Figures 1.6(a)-(b) shows a 3 gore lobe of a 27 gore design and Figures 1.7 shows the complete shape.

Let $V_l, V_{ml}, V_{m'}, V_m, V_{mr}, V_r$ denote vertices along a circumferential fiber at the ith station of Gore-j in the flat reference configuration. Let $v_l, v_{ml}, v_{m'}, v_m, v_{mr}, v_r$ be the corresonding vertices in the deformed configuration. Note that $V_{m'}$ and V_m are the same material point. Vertices $v_{m'}, v_m$ represent the end location of the respective left-half and right-half circumferential fibers (if these fibers were to be extended in a straight line). Vertices of the type v_{mr} and v_r have three degrees of freedom (DOF). Vertices of the type v_{ml} and v_l have 0 DOF, since v_{ml} is equal to v_{mr} on Gore-j and v_l in Gore-j is equivalent to v_r in Gore-$j+1$. Vertex $V_{mr} = (Y_{mr}, Z_{mr})$ has one DOF, since Y_{mr} is allowed to vary between Y_m and Y_r. Similarly, V_{ml} has 1 DOF. Vertices in the form $v_{m'}$ and v_m are determined as follows:

$$v_m = \begin{cases} v_{mr}, & Y_{mr} \le Y_m, \\ v_{mr} + (v_{mr} - v_r)\cdot\tau(V_m, V_{mr}, V_r), & Y_m < Y_{mr} < Y_r, \\ (x_{mr} - (Y_r - Y_m)\cos(\pi/q), y_{mr} - (Y_r - Y_m)\sin(\pi/q), z_{mr}), & Y_{mr} \ge Y_r, \end{cases}$$

Table 1.5: Design Parameters for a 27 gore balloon

Parameter	Description	Design Value
b_d	Buoyancy	1.9459e-02 lbf/ft^3
L	Payload	107 lbf
w_f	Film weight density	0.00384 lbf/ft^2
w_t	Tape weight density	0.00301 lbf/ft
n_g	Number of gores	27
V_d	Volume	5968.46 ft^3
ℓ_d	Gore length	36.0028 ft
θ_0	Angle at base	51.44 deg
$\max Z_d$	Balloon Height	22.935 ft
$2 \cdot \max R_d$	Diameter	23.764 ft
A_T	Surface Area	1617.29 ft^2
W_T	Gross Weight	116.136 lbf

Figure 1.5: A segment of a gore in the reference configuration.

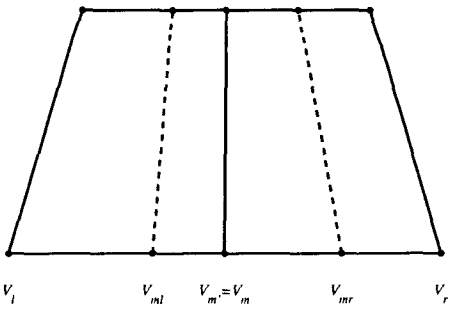

Figure 1.6: LEM-shape at $V = 0.15\,V_d$ for a 27 gore design. (a) Inside view of 3-gore lobe; (b) Outside view of a 3-gore lobe.

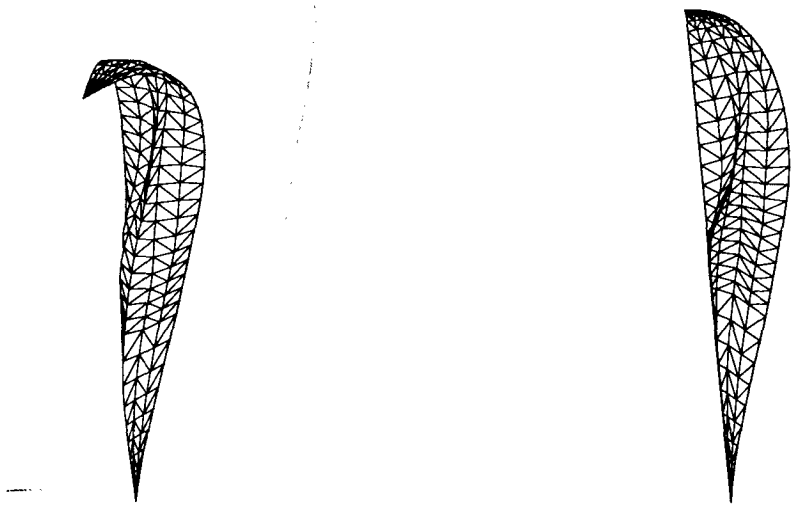

Figure 1.7: A complete LEM-shape at $V = 0.15\,V_d$ for a 27 gore design with nine lobes.

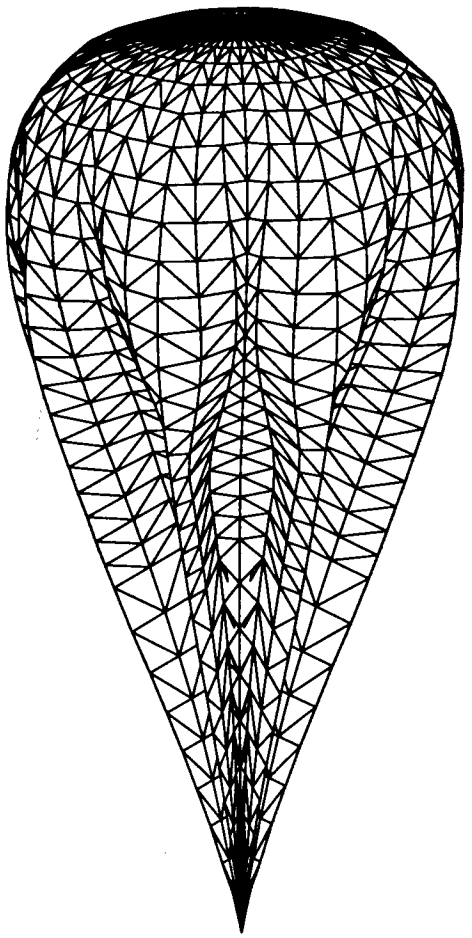

$$v_{m'} = \begin{cases} (x_{ml} - (Y_l - Y_{m'})\cos(\pi/q), y_{ml} - (Y_l - Y_{m'})\sin(\pi/q), z_{ml}), & Y_{m'} \le Y_l, \\ v_{ml} + (v_{ml} - v_l)\cdot\tau(V_{m'}, V_{ml}, V_l), & Y_l < Y_{ml} < Y_{m'}, \\ v_{ml}, & Y_{ml} \ge Y_{m'}, \end{cases}$$

where $\tau(V_m, V_{mr}, V_r) = (Y_{mr} - Y_m)/(Y_r - Y_{mr})$, and $\tau(V_{m'}, V_{ml}, V_l) = (Y_{ml} - Y_{m'})/(Y_r - Y_{mr})$. The vertex that lies at the top of the balloon has one DOF, since it can vary along the z axis only. Linear equality constraints for the bounding planes of a fundamental section S_F are in the form:

$$y_{mr} = 0, \tag{1.52}$$

$$y_r - \tan(\pi/q)x_r = 0. \tag{1.53}$$

For lobed shapes, we impose the condition, $0 \le y \le \tan(\pi/q)x$, for vertices (x, y, z) with non-zero degrees of freedom that are not constrained by Eqs. (1.52)-(1.53). These conditions insure that a balloon shape will have D_q-symmetry. The variational principal for an energy minimizing balloon shape is to minimize the total energy of the balloon system subject to a volume constraint over a class of shapes C_q that incorporates geometry, symmetry, folds, etc. Next, we write out explicitly the terms in the variational principal. To simplify notation, we use S to denote both the actual surface and its approximation. The lth triangle of the jth gore in the reference configuration is denoted by T_l^j and the corresponding triangle in the deformed configuration is denoted by T_l^j. The reference configuration is $S_F = \cup_{j=1}^r \cup_{l=1}^N T_l^j$ and the deformed configuration is $S_F = \cup_{j=1}^r \cup_{l=1}^N T_l^j$. The total number of facets in a typical gore is N. The total number of facets in a typical gore that lie on the outside of the balloon is N^o. The current target volume is V. Components of the total energy of the balloon system contributed by the jth gore of S_F are:

(a) Hydrostatic Pressure:

$$E_{gas}^j = -b\sum_{l=1}^{N}\int_{T_l^j}\tfrac{1}{2}z^2\vec{k}\cdot d\vec{A},$$

(b) Film Weight:

$$E_{film}^j = w_f\sum_{l=1}^{N}\bar{z}_l^j\omega(T_l^j)\text{area}(T_l^j),$$

(c) Tape Weight:

$$E_{tapes}^j = w_t\sum_{i=1}^{n_c+1}\bar{z}_{i,2}^j|E_i^j|,$$

(d) Top Fitting Weight:

$$E_{top} = w_{top}z_{top},$$

(g) Aerodynamic Drag:

$$E_{drag}^j = -\tfrac{1}{2}\rho_{air}C_D v_D^2\sum_{l'}\text{area}\left(\text{Pxy}[T_{l'}^j]\right),$$

where $\mathsf{P}_{\mathbf{xy}}[T]$ is the projection of facet T onto the xy-plane and the summation in l' is over all facets with unit normal making an angle less than $\pi/2$ with the $-\mathbf{k}$ direction (see Eq. (A.3),

(e) Tape Strain:

$$S^j_{tapes} = \tfrac{1}{2}K_t \sum_{i=1}^{n_c+1} (\varepsilon^j_i)^2 |E^j_i|,$$

(f) Film Strain:

$$S^j_{film} = 2\sum_{l=1}^{N} \omega(T^j_l)\mathbf{n}(T^j_l) : \gamma(T^j_l)\text{area}(T^j_l).$$

The volume is $V^j = 2\sum_{l=1}^{N^o} V^j_l$, where n_c is the number of circumferential fibers, w_f is the film weight density, $\omega(T)$ is the number of film layers in facet T, $\bar{z}^j_l$ is the centroid of T^j_l, w_t is the tape weight density, K_t is the tape stiffness, $\mathbf{n}$ is the Second Piola-Kirchoff stress, γ is the Green strain, ε^j_i is the strain in the ith segment of the jth load tape, $\bar{z}^j_{i,2}$ is the centroid of the ith meridional segment in the jth load tape, $|E^j_i|$ is the length of the ith segment of the jth load tape, b is the buoyancy, V^j_l is the volume contribution due to facet l of Gore-j. The height of the top fitting above the base of the balloon is z_{top} and its weight is w_{top}. Summing the contributions over all gores within a lobe and multiplying by q, we obtain the energy of the complete balloon:

$$E_{Total} = q\sum_{j=1}^{r}\left(E^j_{gas} + E^j_{film} + E^j_{tapes} + E^j_{drag} + S^j_{tapes} + S^j_{film}\right) + E_{top}, \tag{1.54}$$

and the volume constraint: $V = q\sum_{j=1}^{r} V^j$. When $r = 1$, we call a shape S that minimizes E_{Total} an *energy minimizing shape* (EM-shape). When $r > 1$, the shape has lobes and we refer to it as a lobed EM-shape (LEM-shape).

1.3 Two-dimensional potential flows

In this section, we consider two dimensional uniform flow around an axisymmetric balloon shape. Bernoulli's Law can be used to compute a pressure distribution.

1.3.1 Potential flow and the PDE Toolbox

In Fig. 1.8(a), we present the profile of a natural shape balloon (near full inflation) and in Fig. 1.8(b), we present a partially inflated natural shape (at roughly 5%-inflation). We assume that the balloon is stationary and far away from the balloon, the fluid moves parallel to the x-axis at a speed of about 4 m/sec

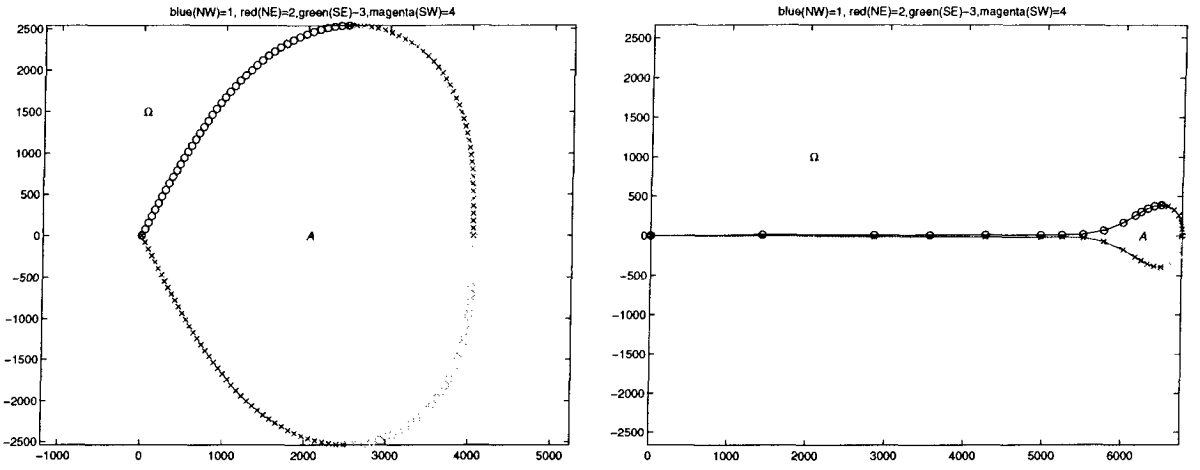

(a) (b)

Figure 1.8: Axisymmetric balloon profiles: (a) full inflation; (b) 5% inflation

Let B be the rectangle, in the xy-plane,

$$B = \{(x,y) \mid L_1 \leq y \leq L_3,\ L_2 \leq x \leq L_4\}$$

and $\partial B = \partial B_1 \cup \partial B_2 \cup \partial B_3 \cup \partial B_4$, where

$$\begin{aligned} \partial B_1 &= \{(x,y) \in B, y = L_1\}, \\ \partial B_2 &= \{(x,y) \in B, x = L_2\}, \\ \partial B_3 &= \{(x,y) \in B, y = L_3\}, \\ \partial B_4 &= \{(x,y) \in B, x = L_4\}, \end{aligned} \tag{1.55}$$

where $L_1 + L_3 = 0$.

Let A denote the interior of the balloon shape (see Fig. 1.8), and let Ω be the region exterior to A, but interior to B:

$$\Omega = B \setminus A.$$

In Fig. 1.9(a) and Fig. 1.9(c), we present a discretization of the region Ω produced using the PDE Toolbox that is exterior to the balloon for full and 5% inflation, respectively. The initial meshes can be refined by the user or adaptively refined by PDE Toolbox (see Fig. 1.9(b) and (d)). For the purpose of this exposition, we impose Neumann boundary conditions on $\partial B_2 \cup \partial B_4$, and Dirichlet boundary conditions on ∂A and $\partial B_1 \cup \partial B_3$. We are led to the following boundary value problem:

$$\textbf{(BVP)} \qquad \begin{aligned} \triangle \psi &= 0, \text{ on } \Omega, \\ \psi &= 0, \text{ on } \partial A, \\ \frac{\partial \psi}{\partial n} &= 0, \text{ on } \partial B_2 \cup \partial B_4, \end{aligned}$$

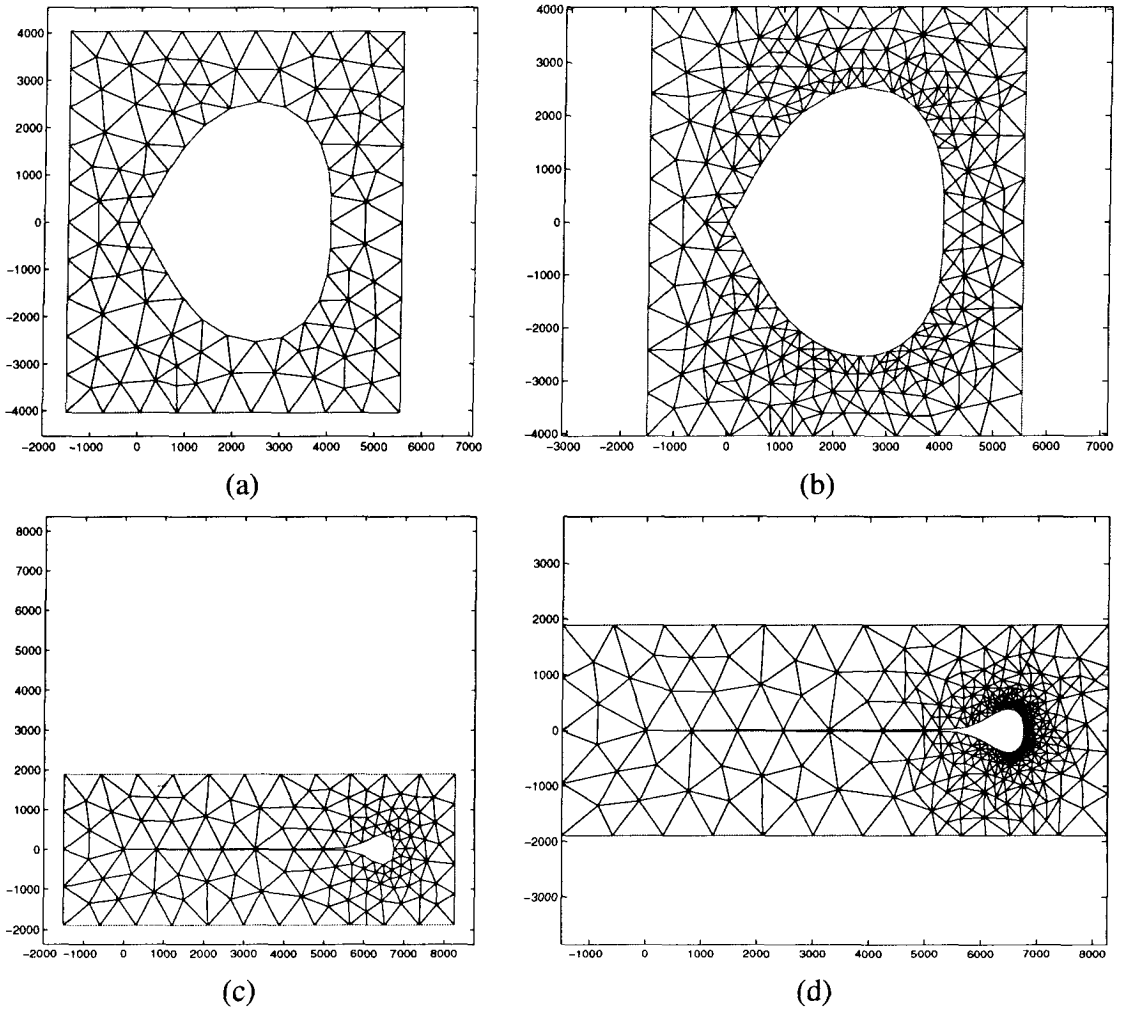

Figure 1.9: From PDE Toolbox (a) Initial mesh for full inflation shape; (b) Adapted/refined mesh for full inflation shape; (c) Initial mesh for 5% inflation shape; (d) Adapted/refined mesh for 5% inflation shape.

$$\begin{aligned} \psi &= -\psi_0, \text{ on } \partial B_1, \\ \psi &= \psi_0, \text{ on } \partial B_3, \end{aligned}$$

where ψ is the stream function, and $\partial/\partial n$ is the normal derivative. In this case, the velocity field is

$$\mathbf{v} = \frac{\partial \psi}{\partial y}\mathbf{i} - \frac{\partial \psi}{\partial x}\mathbf{j}. \tag{1.56}$$

The PDE Toolbox can be used to solve BVP, compute the velocity field, and to plot the corresponding flow lines on the adapted mesh. The results are shown in Fig. 1.10. Under the assumption of steady irrotational flow of a fluid with uniform density ρ, we have the following

$$\frac{P}{\rho} + \tfrac{1}{2}|\mathbf{v}|^2 = \text{Constant}, \tag{1.57}$$

from which we can determine the pressure P; $\mathbf{v}$ is the velocity field (see Eq. 1.56). Eqn. (1.57) is called Bernoulli's Law.

1.3.2 Concluding remarks

The PDE Toolbox is restricted to two dimensional flows, and we would have difficulties extending this approach to a flow problem for a balloon with lobes. As outlined in Chapter 2, the methods in Chapter 1 can be extended to full three dimensional problems. Drag is most likely the dominant aerodynamic load for the inflation/deployment phase of a planetary balloon mission and so it makes sense to develop further the methods of Chapters 1–2.

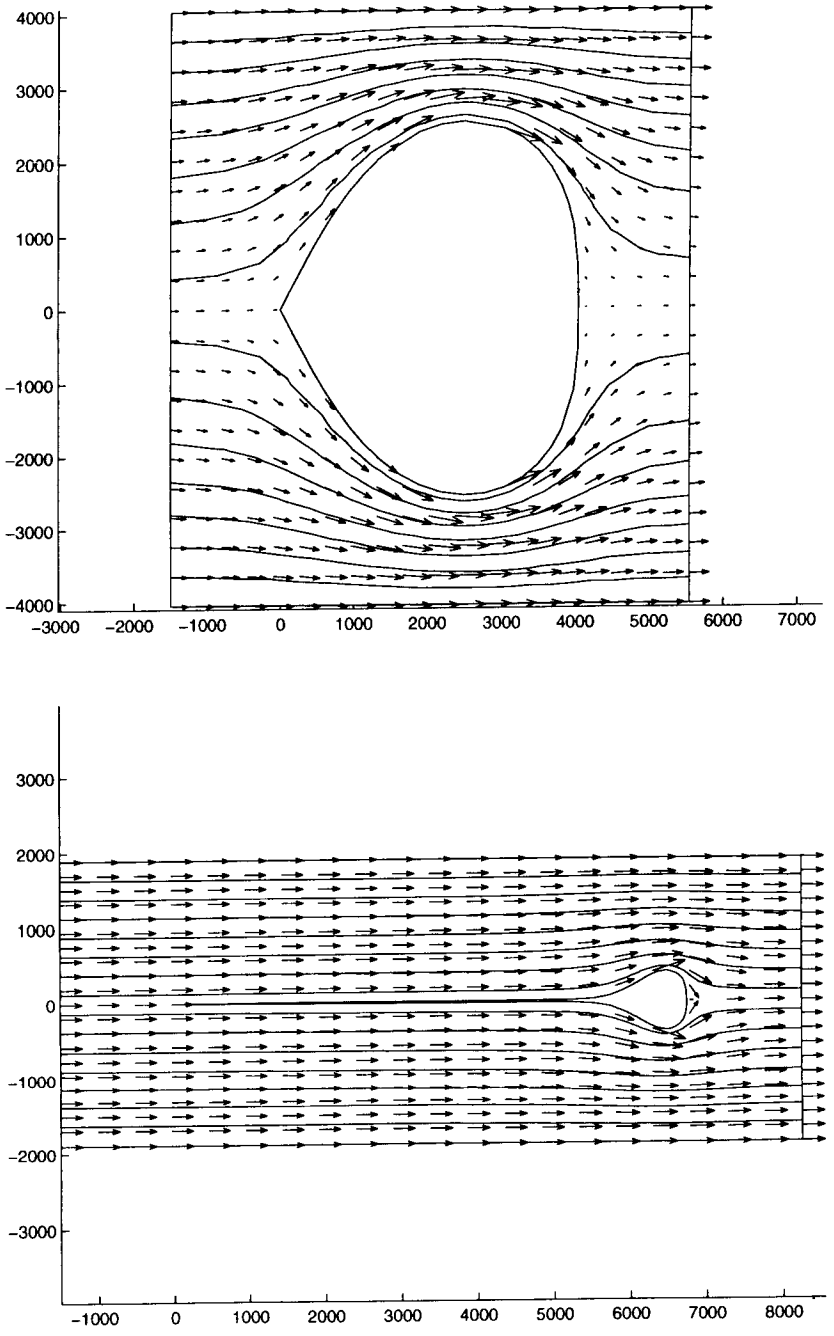

Figure 1.10: Velocity field and flow lines: (a) Full inflation; (b) 5% inflation

1.4 Dynamic model for a descending spherical balloon

In the following, we consider a simple dynamic model for a descending spherical balloon that is inflating with air. The motivation is a Mars solar Montgolfiere balloon. The total force on the balloon is equal to the sum of the lift due to the gas, dead weight of the balloon system (payload and balloon), and drag. In particular, we have (see [7, p. II-15, Eq.(32)])

$$m_v \frac{d^2 z}{dt^2} = F_{Lift} - g(m_B + m_L) + F_D, \quad 0 < t < t_{R_d} \tag{1.58}$$

where

$$\begin{aligned}
z &= z(t) \text{ (altitude of balloon, geopotential height)} \\
t &- \text{time} \\
m_B &- \text{mass of balloon} \\
m_L &- \text{mass of payload} \\
r_o &- \text{radius of intake at base of balloon} \\
m_v &= m_B + m_L + m_g + C_m \rho_a(z) V \text{ (virtual mass)} \\
V &= \pi r_o^2 (z(t) - z_0) + V_0 (V_0 \text{ is the initial fill}) \\
\rho_a &= \rho_a(z) \text{ (density of atmosphere)} \\
R &= \left(\frac{3V}{4\pi}\right)^{1/3} \text{ (radius of sphere with volume } V) \\
A_D &= = \pi \max(R^2, r_o^2) \text{ (frontal area of spherical balloon)} \\
T_a &= T_a(z) \text{ (temperature of atmosphere)} \\
m_g &= m_{g,0} + \pi r_o^2 \int_z^{z_0} \rho_a(H) dH \\
\hat{\rho}_g &= m_g / V \text{ (mean density of gas)} \\
F_{Lift} &= g \rho_a V - g m_g \\
&= g V \rho_a \left(1 - \frac{\hat{\rho}_g}{\rho_a}\right) \\
&= g V \rho_a \frac{\Theta}{T_a + \Theta} \\
F_D &= \tfrac{1}{2} \rho_a(z) C_D \left|\frac{dz}{dt}\right| \frac{dz}{dt} A_D \\
C_D &= 0.8 \text{ (for a descending balloon)} \\
t_{R_d} &- \text{time when the balloon first reaches full inflation, i.e., } R = R_d \\
&\text{Units: Length-meters, Mass-kilograms, Time-seconds}
\end{aligned}$$

Table 1.6: Parameter values for a spherical balloon

Quantity	parameter	Value
Mass of payload	m_L	6 kg
Diameter (at full inflation)	$2R_d$	15 m
Mass of balloon	m_B	5.65 kg
Film density	ρ_f	8 g/m^2
Initial velocity	$v_{B,0}$	-50 m/sec
Supertemperature	Θ	112° K

Table 1.7: Test Case data

Quantity	parameter	Value	
t	z	z'	z''
0	36520	-50	-9.230
87.6	34957	-10.99	0.068
720	30501	-4.06	0.008
1200	29378	-0.712	0.007
2400	29356	-0.030	-0.001

The term $C_m \rho_a(z) V$ is the added environmental mass that is assumed to be accelerated along with the balloon, payload, and gas masses. For balloon applications, one typically assumes $C_m = \frac{1}{2}$ ([7, p.g II-12]). The quantities ρ_a (see Eq. (C.5)) and T_a (see Eq. (C.1)) are discussed in Appendices A-B. For $t > t_{R_d}$, we assume that the balloon maintains a spherical shape with a radius of $R = R_d$, and terms in Eq. (1.58) can be appropriately modified.

Next, we consider a test case based on the values presented in Table 1.6. When released, we assume that the balloon is falling with a velocity of -50 m/sec. At the altitude where the balloon is fuly inflated, we assume that the atmospheric pressure is 0.00827 mb; this corresponds to an altitude of 34957 m. We estimate that the balloon must fall 1563 m in order to reach full inflation, and so we assume the release altitude is 36520 m. Integrating the Eqn. (1.58) with the iniital conditions of $z'(0) = -50$ and $z(0) = 36520$, we find that it takes 87.6 sec for the falling balloon to inflate, i.e. $t_{R_d} = 87.6$). After full inflation, $z'(87.6) = -10.99$ m/sec., $z''(87.6) = 0.068$ m/sec^2. Other values of z, z', z'' are displayed in Table 1.7. After about 720 sec, the balloon reaches is minimum altitude and begins slowly oscillating about some mean altitude. In Figure 1.11, we present data related to the U.S. Standard Atmosphere. In Figure 1.12, we present plots of $(t, z(t))$ and $(t, z'(t))$ for $0 < t < t_{R_D}$.

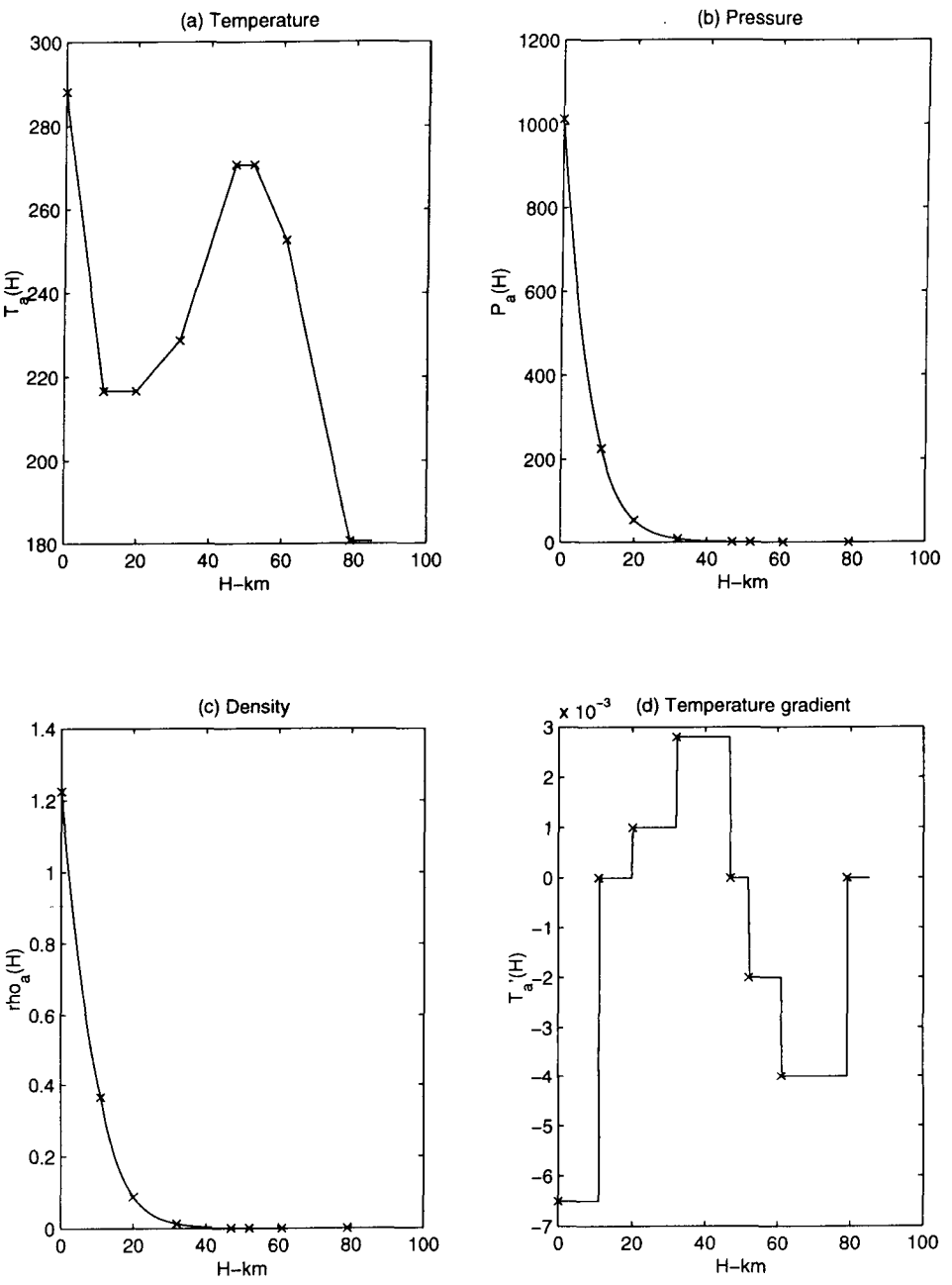

Figure 1.11: Atmosphere related plots; (a) T_a - temperature; (b) P_a - pressure; (c) ρ_a - density; (d) T_a' - temperature gradient.

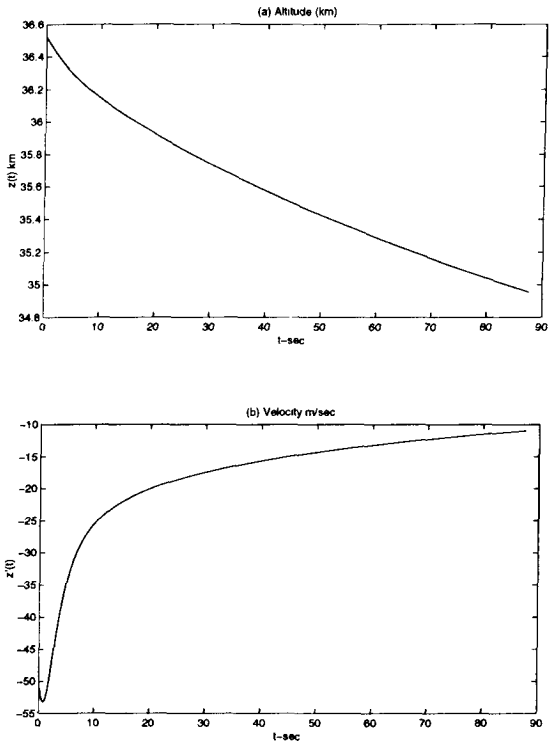

Figure 1.12: Altitude and velocity from test case; (a) $z(t)$ - altitude; (b) $z'(t)$ - velocity.

1.5 General Remarks on Aerodynamic Loading

The methods outlined in Chapters 1-2 are feasible approaches to incorporating aerodynamic loading into balloon shape analysis. While the natural shape model described in Chapter 1 does not include elasticity, it provides a good first step for determining the effects of aerodynamic loading. The approach outlined in Chapter 2 can be adapted to nonaxisymmetric shapes and fits very naturally in our program for modeling partially inflated balloon shapes by variational techniques and energy minimization.

Adding these aerodynamic capabilities to our LEM-model, we would be able to provide analytical capabilities that could be used to support missions such as the Mars Solar Montgolfiere Balloon that is being studied by JPL, especially for the critical inflation/deployment phase. These capabilities could also be applied to ultra long duration flights, including in-spool configurations, constrained ascent shapes, and ascent shapes. While the analytical results of Chapter 1 are related to axisymmetric shapes, with capabilities that are now being developed in LEMsolver and the approach outlined in Chapter 2, we should be able to develop a tool for analyzing aerodynamically loaded balloons for a variety of configurations.

Chapter 2

Lobed Balloon Shapes

A feature characterizing partially inflated scientific balloons is a lobe structure surrounding the gas bubble. We present a mathematical model for such a balloon shape. We formulate a variational principal for the balloon system, and seek to determine a shape that minimizes energy subject to a volume constraint. The energy includes film and load tape strain, film and load tape weight, and hydrostatic pressure. Numerical solutions are presented for a 24-gore balloon with and without lobes.

2.1 Introduction

Ascent shapes of large scientific balloons are characterized by the formation of lobes surrounding the gas bubble. Based on observations of real balloons, it is reasonable to assume that these structures are periodic. Balloon shapes with lobes were investigated in [5] using variational techniques where the energy of the balloon system included hydrostatic pressure and film weight. The energy of the balloon system was minimized subject to constraints on the volume and the lengths of certain fibers. Geometrically, the shapes in [5] possessed many features seen in real balloons: lobes surrounding the gas bubble, a sphere-like top, internal folds of excess balloon fabric, and flat wing-like structures (fins) hanging beneath the gas bubble. However, the formulation of the problem did not include strain energy. In [2] and [4], the film and load tape strain energies were considered for shapes modeled by a half-gore. In the present work, we formulate a variational principal for a partially inflated balloon in such a way that a lobed structure can (but not necessarily) form. Based on observations, it appears that a lobed shape is somehow preferred over a cyclic shape without lobes when the volume is significantly less than the float volume.

Applying our model to a representative shape (a 24-gore balloon design), we investigate by parametric studies the existence of a minimum energy selection principal behind the formation of

lobes in balloon shapes. In addition, we compare various quantities such as total energy, strain energy, and maximum principal stress resultants for balloon shapes with a different number of lobes. When there are a large number of gores per lobe, we found that shapes with self-intersections could evolve. By monitoring the evolution of a family of LEM-shapes and (when necessary) adding a perturbation to break the symmetry, we found that in the cases studied, the self-intersection could be avoided.

In the following, we let $S(V,q)$ denotes a deformed balloon with volume V and q lobes. The number of gores per lobe is p and the total number of gores is $n_g = pq$. If it is clear from context, we will omit certain arguments and write S instead of $S(V,q)$. S_F denotes a fundamental section of S (S_F is centered about a vertical plane of reflectional symmetry). In the past, we assumed that p was odd. However, in this treatment, we will only require that q divides n_g. A superscript $j = 1,2,\ldots,p$ will be used to denote a quantity that is related to the jth gore of S_F. When $p = 1$, the balloon shape can be modeled by a half-gore. When $p > 1$, the balloon can have lobes. Viewed from above, a design shape will have the symmetries of a regular polygon with n_g sides. In general, $S(V,q)$ will be invariant under the dihedral group D_q. Viewed from above, $S(V,q)$ will have the symmetries of a regular polygon with q sides. The set of balloon shapes invariant under D_q will be denoted by C_q. To demonstrate our approach, we will consider a natural-shape design with $n_g = 24$, noting[1]

$$C_{24} \subset C_{12} \subset C_6 \subset C_3 \text{ and } C_{24} \subset C_8 \subset\subset C_4. \tag{2.1}$$

We compute a family of balloon shapes with D_{24} symmetry and a family of balloon shapes with D_k symmetry and $k = 24,12,8,6,4,3$ The numerical solutions we present here need not be all the possible solutions. In Table 2.1, we list the combinations of p and q that are possible for a 24-gore balloon. Table 2.1 contains design shape parameter values. Before we present our mathematical model, it is a good to have a rough idea of the geometry of a partially inflated shape for various inflation levels. Beginning at float altitude, we assume $V = V_d$ (its design volume). At float, the balloon envelope is fully deployed. As the volume decreases, the balloon becomes taller and narrower. Shapes of this kind can be modeled by a half-gore and were the focus of [4]. For $0.6V_d < V < V_d$, we see that as the volume decreases, each deformed gore moves toward the z-axis and an internal fold of excess material forms in the center of the gore. In an internal fold, the exterior of the balloon comes into contact with itself. To reduce the number of unknowns, in our treatment here, we will not use an explicit model of the internal fold. For a sufficiently small volume, the inside of the balloon will come into contact with itself. Since the precise nature of the

[1] In the variational formulation of the balloon problem, the energy of the balloon shape will be minimized over some C_q. However, due to Eq. (2.1)), it is possible in certain cases that a shape $S_{q'}$ with $q' > q$ to evolve when minimizing over S_q. If this does happen, we can add a perturbation to an intermediate shape in order to break the $D_{q'}$ symmetry.

Gores per Lobe	Number of Lobes
p	q
1	24
2	12
3	8
4	6
6	4
8	3
12	2

Table 2.1: Parameter values for balloon

E (psi)	ν	w_f (lbf/in^2)	w_t (lbf/in)	K_t (lbf)	e (in)	b_d (lbf/in^3)	V_d (in^3)	n_g	ℓ_d (in)	w_{top} (lbf)
36000	0.82	2.667e-05	2.50833e-04	2810	0.0008	1.1330556e-05	10775165.571	24	433.15	1.5

distribution of folded material is unknown, we can still compute balloons shapes at small volumes with D_{24} symmetry. However, when $V << V_d$, it may not be reasonable to continue to assume that D_{24} symmetry is preserved, because of the bulk of excess balloon material hanging at the base of the balloon will prevent this from happening. Furthermore, there may be many other factors that influence symmetry breaking, load tape slackness (length variation), gore size variation, folding of the balloon stack, and other variations introduced while the balloon is in the launch spool.

2.2 Mathematical Model

In the numerical calculations presented here on strained lobed balloon shapes, we will use the expression for the total energy E_{Total} as given by (1.54) and $C_D = 0$ (no aerodynamic loading). Furthermore, we will make the assumption that $v_{ml} = v_{m'} = v_m = v_{mr}$. This will significantly reduce the number of degrees of freedom, but we can still obtain reasonable estimates for the maximum film stresses

2.3 Numerical results and discussion

Figures 2.1- 2.2 suggest that the total energy of a balloon shape is essentially independent of the number of lobes when $0.5\,V/V_d < 1$. For shapes near $V/V_d = 0.2$, it appears that shapes with 6 or 12 lobes have a total energy about 3.5% less than the other shapes for that same volume (see

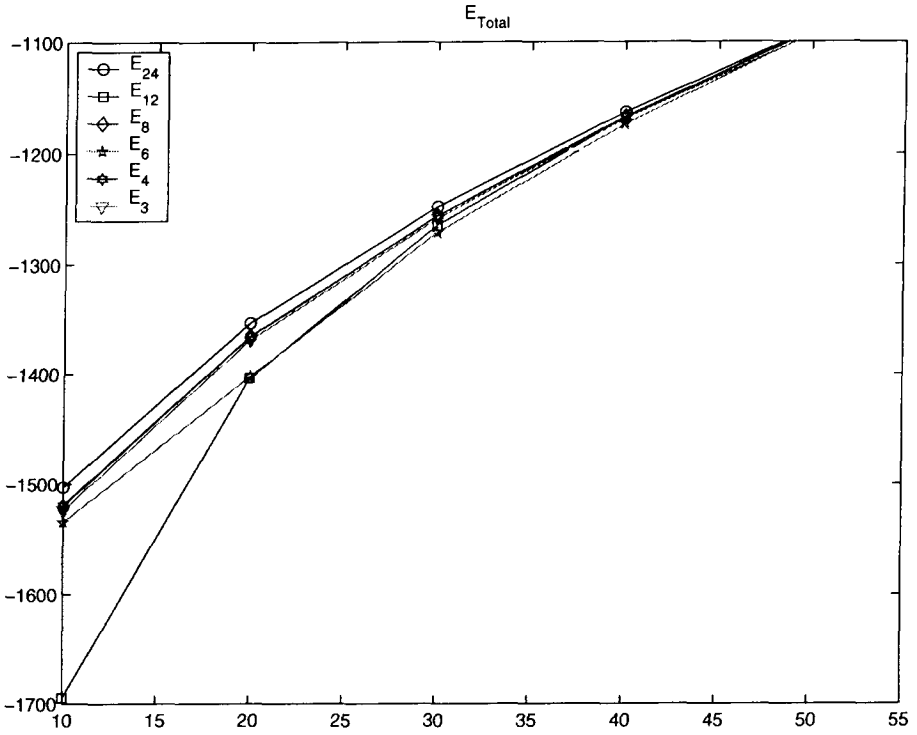

Figure 2.1: Total energy for lobed shapes at $V/V_d = 0.1, 0.2, 0.3, 0.4, 0.5$ (Units of energy lbf-in.

Figure 2.1). Geometrically, the shapes S_6 and S_{12} are very similar. In S_6 there are two flat wings per lobe, leading to a total of 12 lobes. There is a similar pairing of the shapes, S_4 with S_8 and S_3 with S_6.

Remark These results suggest that it might be relatively easy for a strained partially inflated lobed zero-pressure balloon to transition from a state with n-lobes to one with $n+k$ lobes. It would be of interest to study the stability of these shapes and to carry out a similar study for partially inflated pumpkin balloons. This could shed some light on problems associated with the ascent and deployment of pumpkin balloons.

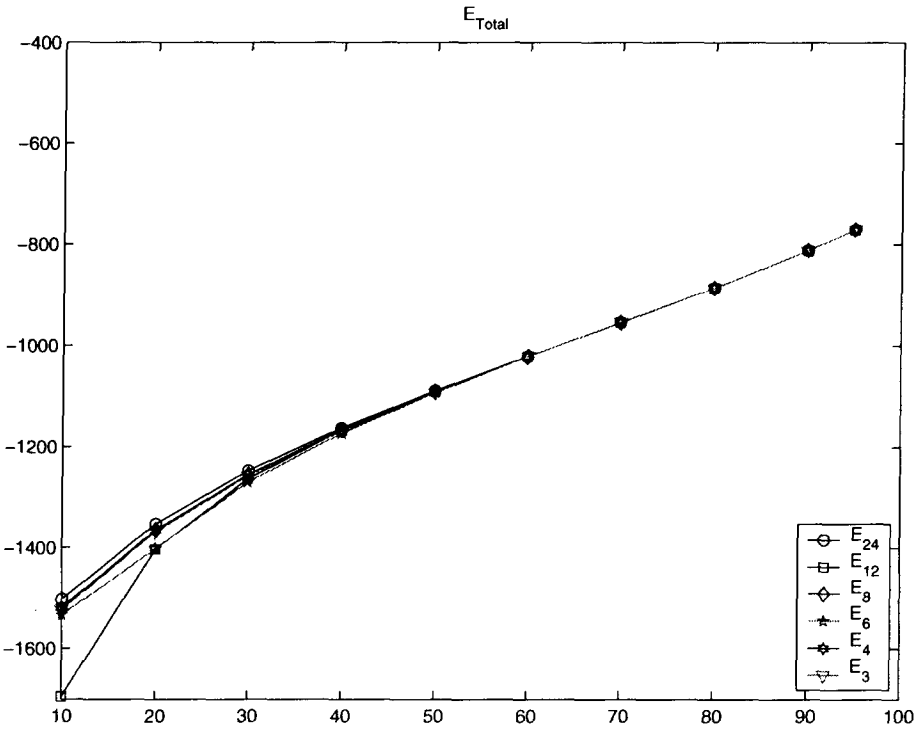

Figure 2.2: Total energy for lobed shapes at $V/V_d = 0.1, 0.2, 0.3, 0.4, 0.5$ (Units of energy lbf-in.

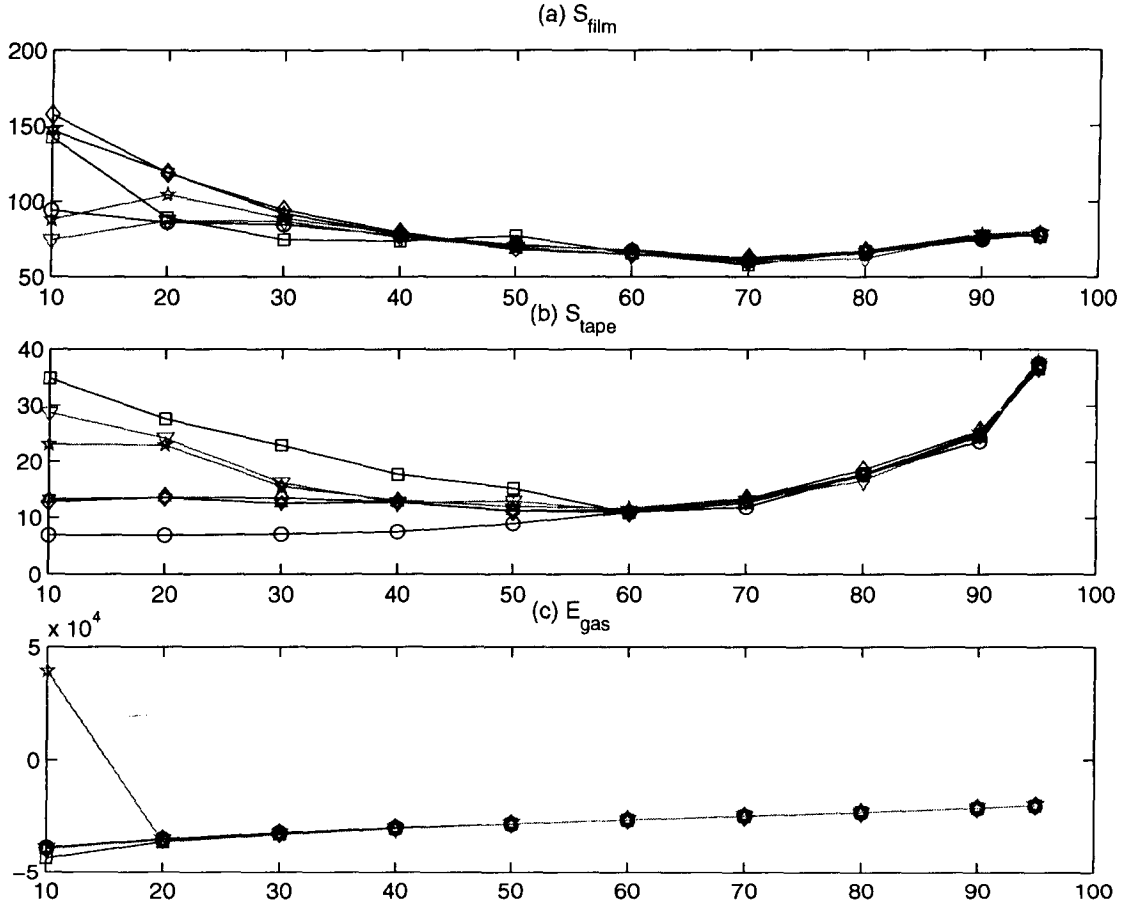

Figure 2.3: Lobed balloon shapes at $V/V_d = 0.1, 0.2, 0.3, \ldots, 0.9, 0.95$. (a) Film strain energy; (b) Tape strain energy; (c) Hydrostatic pressure potential;

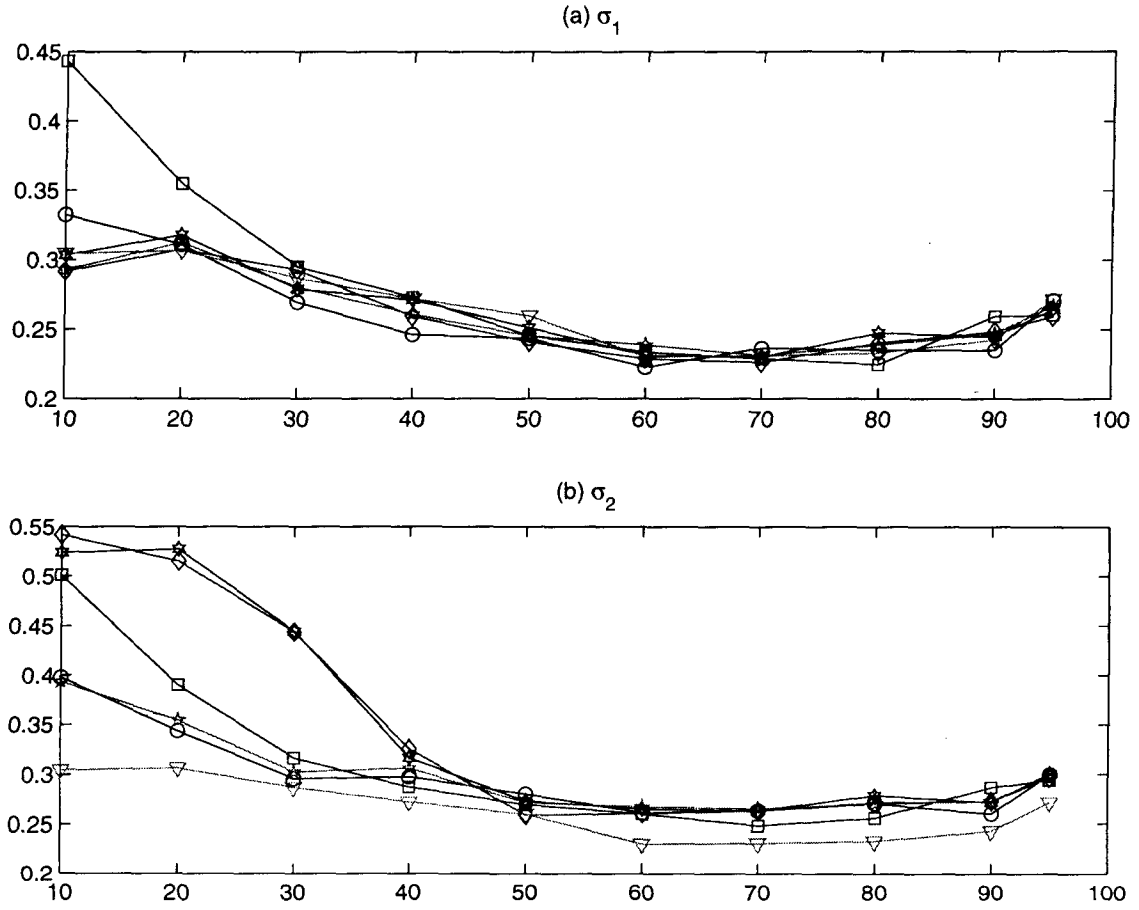

Figure 2.4: Lobed balloon shapes at $V/V_d = 0.1, 0.2, 0.3, \ldots, 0.9, 0.95$. (a) Max principal stress resultant - σ_1 (lbf/in); (b) Max principal stress resultant - σ_2 (lbf/in).

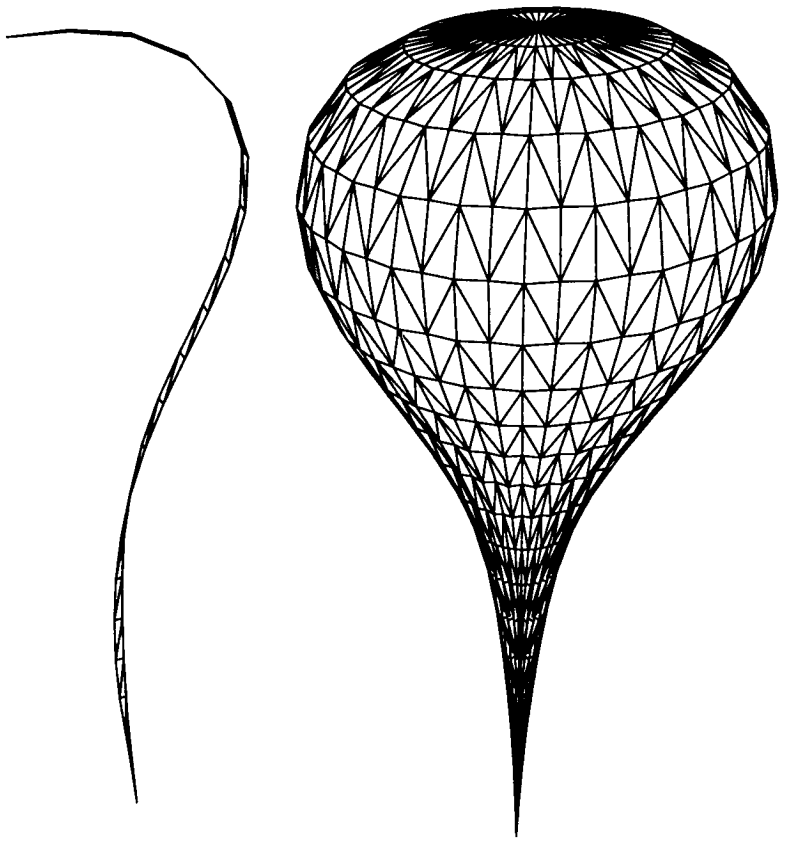

Figure 2.5: 24-gore balloon: 24 lobes/1 gore per lobe

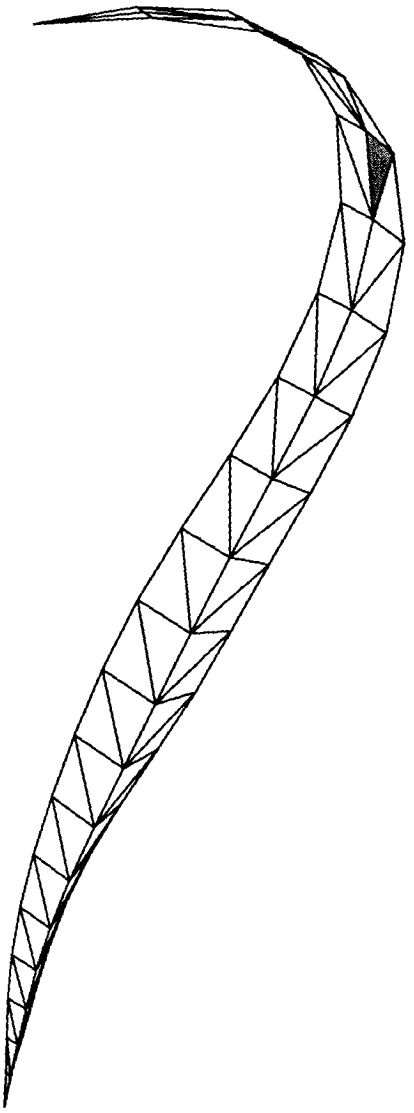

Figure 2.6: 24-gore balloon: 12 lobes/2 gores per lobe

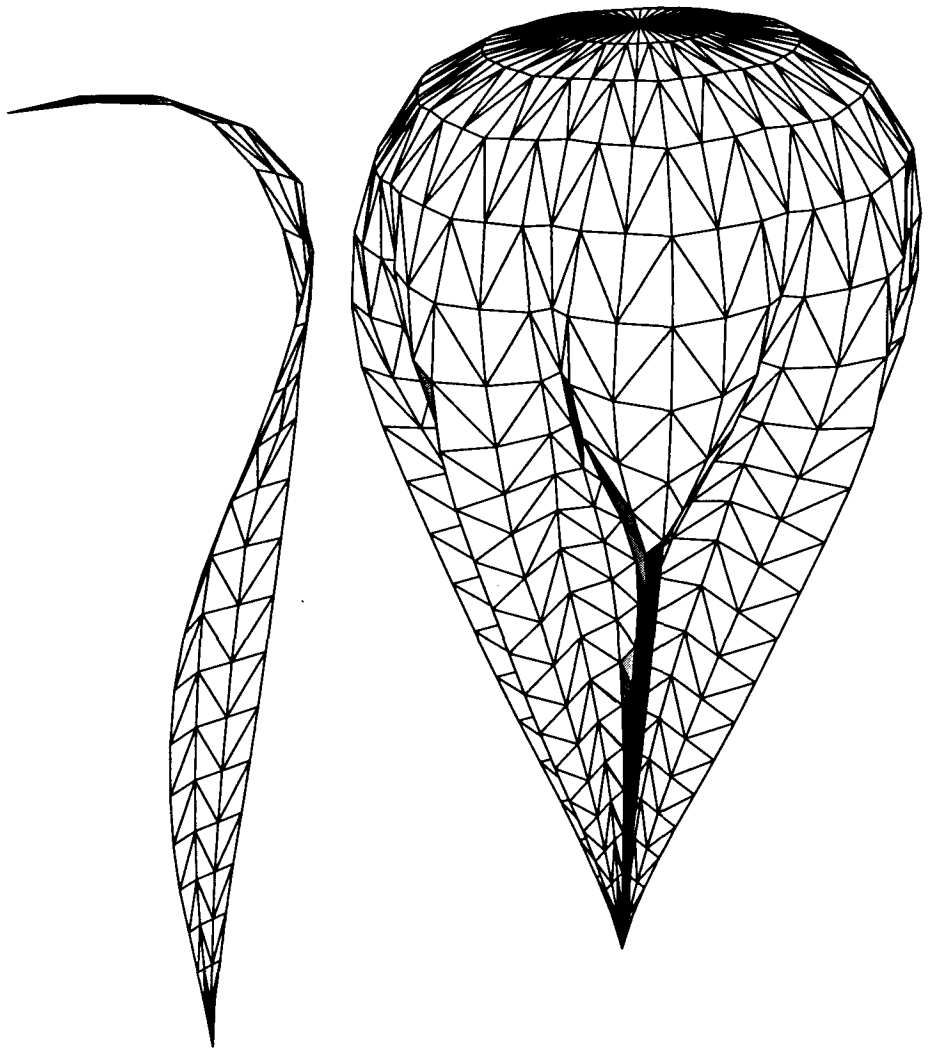

Figure 2.7: 24-gore balloon: 8 lobes/3 gores per lobe

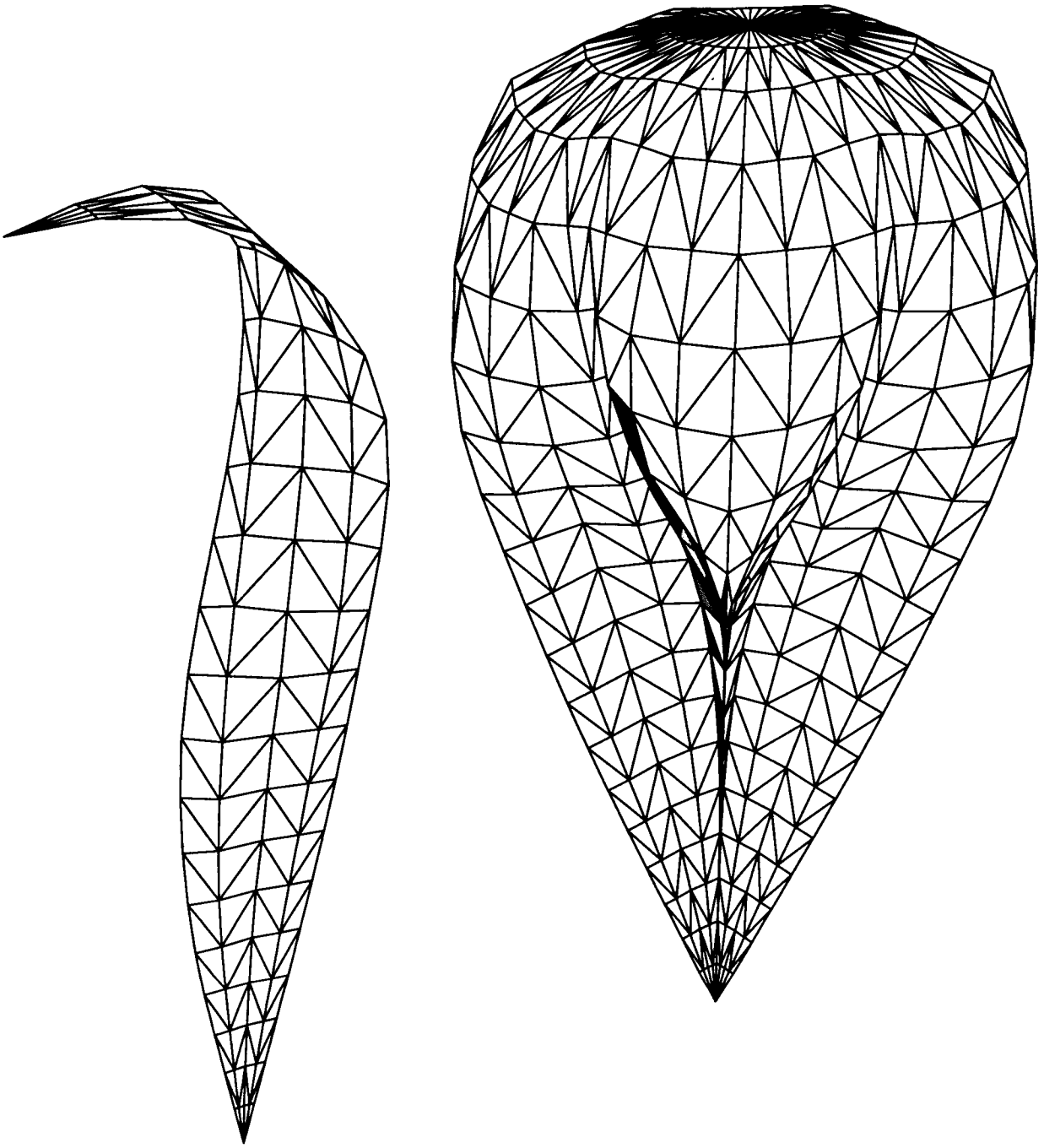

Figure 2.8: 24-gore balloon: 6 lobes/4 gores per lobe

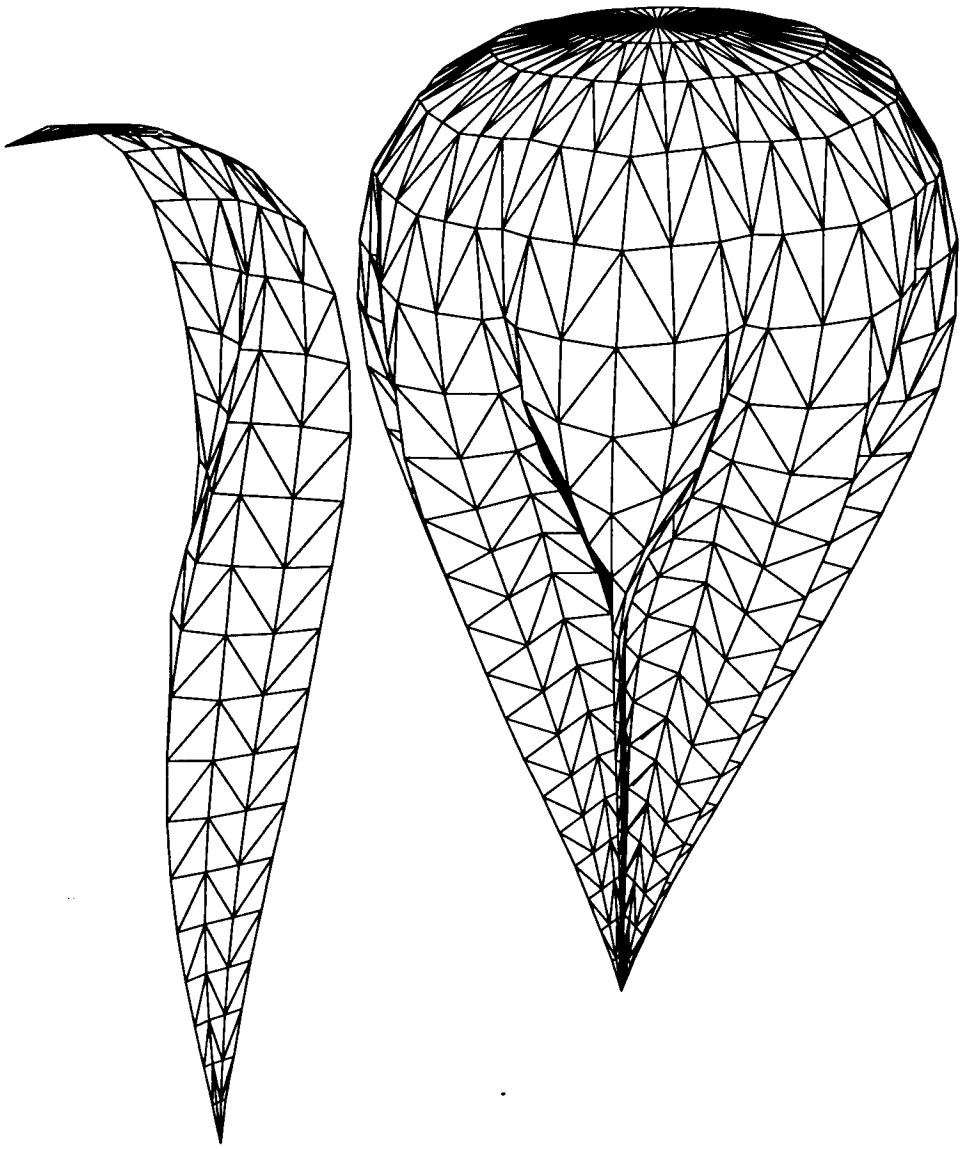

Figure 2.9: 24-gore balloon: 4 lobes/6 gores per lobe

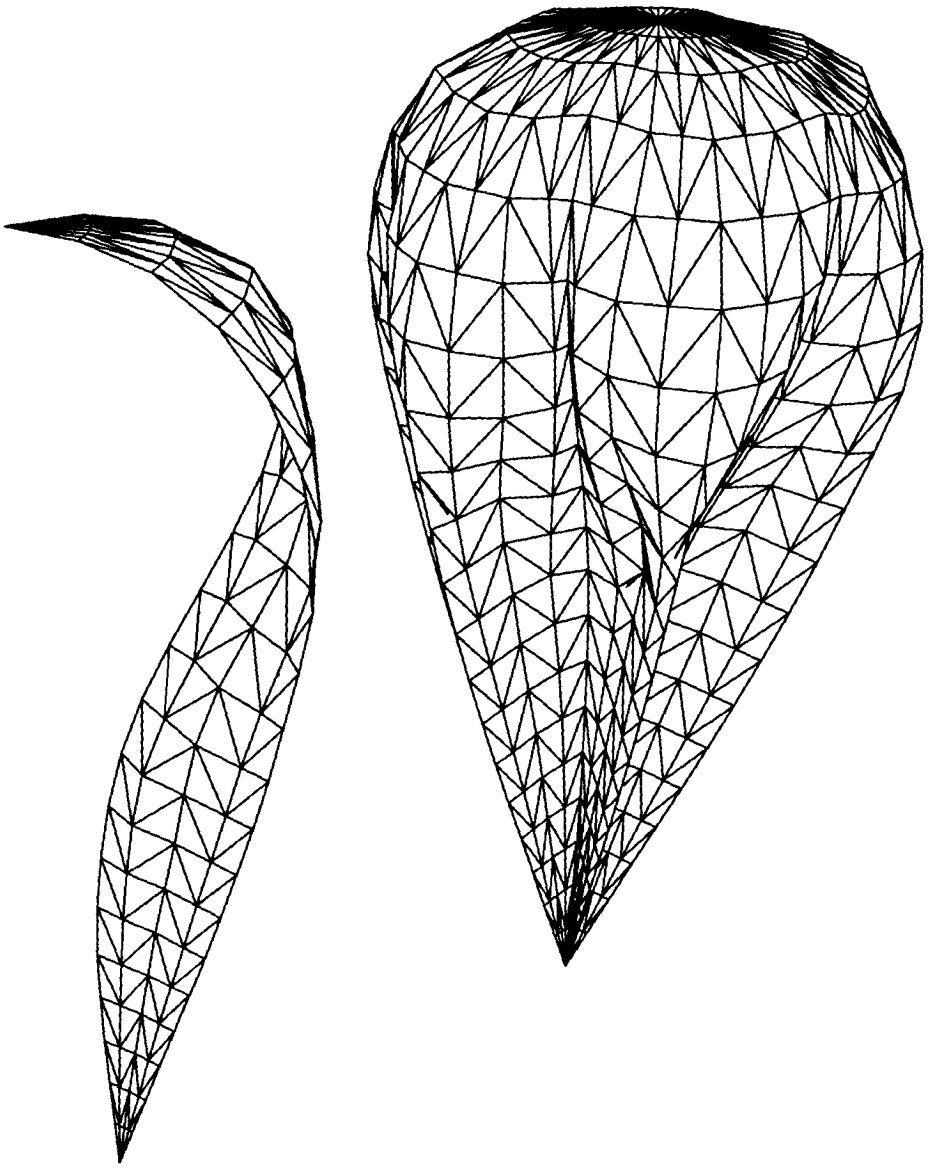

Figure 2.10: 24-gore balloon: 3 lobes/8 gores per lobe

Bibliography

[1] ANON., *Research Development in the Field of High Altitude Plastic Balloons*, NONR–710(01a) Reports, Department of Physics, University of Minnesota, Minneapolis, Minnesota, 1951–1956.

[2] F. BAGINSKI, AND W. COLLIER , *A mathematical model for the strained shape of a large scientific balloon at float altitude*, ASME J. of Appl. Mech., **67** No. 1 (2000), 6-16.

[3] F. BAGINSKI, W. COLLIER AND T. WILLIAMS, *A parallel shooting method for determining the natural-shape of a large scientific balloon*, SIAM J. Appl. Math., Vol. 58, pp. 961-974, June 1998.

[4] F. BAGINSKI & K. BRAKKE, *Modeling ascent configurations of strained high altitude balloons*, AIAA J., Vol. 36, No. 10 (1998), 1901-1910.

[5] F. BAGINSKI, *Modeling nonaxisymmetric off-design Shapes of large scientific balloons*, AIAA Journal, 34 Number 2 (1996), pp. 400-407.

[6] COLLIER, W., *Estimating stresses in a partially inflated high altitude balloon using a relaxed energy approach*, to appear in the Q. of Appl. Math.

[7] A.L. MORRIS (ED.), *Scientific Ballooning Handbook*, NCAR-TN-99, National Center for Atmospheric Research, Boulder, Colorado, May, 1975.

[8] Pipkin, A.C., *Relaxed energy densities for large deformations of membranes*, IMA Journal of Applied Mathematics, 52, pp. 297-308, 1994.

[9] J.C. WARREN, J. H. SMALLEY, & A. L. MORRIS, *Aerostatic Lift of Helium and Hydrogen in the Atmosphere*, NCAR-TN/IA-69, NCAR Technical Notes, National Center for Atmospheric Research, Boulder, Colorado, December, 1971.

[10] JAMES O. WILKES, *Fluid Mechanics for Chemical Engineers*, Prentice Hall, New Jersey, 1999.

[11] S. S. ANTMAN, *Nonlinear Problems of Elasticity*, Springer-Verlag, New York, 1995.

[12] J. P. CHABARD, B. METIVET, G. POT, AND B. THOMAS, *An efficient finite-element method for the computation of three-dimensional turbulent incompressible flows*, Finite Elements in Fluids, ed. T. J. Chung, Series in Computational and Physical Processes in Mechanics and Thermal Sciences, Vol. 8, Hemisphere Publishing, Washington, 1992.

[13] H.B. KELLER, *Numerical Two-Point Boundary-Value Problems*, Dover, New York, 1982.

[14] H.B. KELLER, *Numerical Methods for Two-Point Boundary-Value Problems*, Blaisdell Publishing Company, Waltham, Massachusetts, 1968.

[15] J. H. SMALLEY, *Determination of the shape of a free balloon* , AFCRL-65-68, Nov. 1964.

[16] J. H. SMALLEY, *Balloon shapes and stresses below the design altitude*, NCAR-TN-25, Minneapolis, Minnesota, Dec. 1996.

Appendix A

Aerodynamic drag

In general, the drag on a submersed body exerted by a fluid that is in motion through the fluid is

$$\mathbf{F}_D = -\tfrac{1}{2}\rho_{air} C_D A_D |\mathbf{v}_B - \mathbf{v}_{air}|(\mathbf{v}_B - \mathbf{v}_{air}), \tag{A.1}$$

where C_D is the drag coefficient, ρ_{air} is the density of the air, A_D is the area of the projection of the body on the plane perpendicular to the direction of motion, $\mathbf{v}_B$ is the velocity of the balloon, $\mathbf{v}_{air}$ is the velocity of the atmosphere (see [7, p. II-13] and [10, Sec. 4.3]). In our applications, the velocity of the balloon will be in the $\pm\mathbf{k}$ directions.

Aerodynamic drag can be introduced into our balloon model by adapting Eq. (A.1) appropriately. Consider an arbitrary facet in the triangulation of a balloon shape that is not part of a fold. Let v_0, v_1, v_2 denote the vertices, and $\vec{e}_0 = v_1 - v_0$, $\vec{e}_1 = v_2 - v_1$, $\vec{e}_2 = v_0 - v_2$. We assume that v_0, v_1, v_2 are ordered in such a way that the unit normal $\mathbf{n} = \vec{e}_0 \times \vec{e}_1 / |\vec{e}_0 \times \vec{e}_1|$ points outward. For a balloon descending with a velocity $\mathbf{v}_B = -v_B\mathbf{k}$, the drag on typical triangle T is:

$$F_D(T) = \begin{cases} -\tfrac{1}{2}\rho_{air} C_D v_B^2 \, \vec{dA} \cdot \mathbf{k}, & 0 < \arccos(-\mathbf{k}\cdot\mathbf{n}) < \pi/2, \\ 0 & \text{else}, \end{cases} \tag{A.2}$$

where $\vec{dA} = \frac{1}{2}|e_0 \times e_1|\mathbf{n}$. Adding up the drag contributions of each facet that contacts the atmosphere yields the total potential energy of the drag on the balloon, i.e.,

$$E_D(S) = -\tfrac{1}{2}\sum_{\ell'} F_D(T_{\ell'}), \tag{A.3}$$

where the summation in ℓ' is over all facets whose normal satisfies $0 < \arccos(-\mathbf{k}\cdot\mathbf{n}) < \pi/2$.

Appendix B

Buoyancy of lifting gas

In this appendix, we summarize the background related to the calculation of the buoyancy b of the lifting gas that is used for the hydrostatic pressure p. While there are numerous parameters and combinations of those parameters that lead to the same b, we will provide some of the basic results here. We follow the conventions in [7] and [9].

Archimedes Principle states that a body submerged in a fluid exerts a force equal to the weight of the displaced fluid. In a balloon, the buoyant force or lift is

$$B = W_a - W_g, \tag{B.1}$$

where W_a is the weight of the displaced air and W_g is the weight of the lifting gas. Furthermore, we have $W_a = g\rho_a V_g$ and $W_g = g\rho_a V_g$ where g is acceleration due to gravity, ρ_a is the density of the air, ρ_g is the density of the lifting gas, and V_g is the volume of the gas. The volume of the gas is nearly the same as the volume of the displaced air. In particular, we have

$$B = gV_g(\rho_a - \rho_g) \tag{B.2}$$

or equivalently

$$B = gV_g\rho_a\left(1 - \frac{\rho_g}{\rho_a}\right). \tag{B.3}$$

From the equation of state, we have

$$\rho = \frac{PM}{RT}, \tag{B.4}$$

where P is pressure, M is molecular weight, T is absolute temperature, and R is the universal gas constant. Using a subscript of 'a' or 'g' for quantities related to air or gas, respectively, we find

$$B = gV_g\rho_a\left(1 - \frac{P_g T_a M_g}{P_a T_g M_a}\right). \tag{B.5}$$

If we assume that

$$\frac{P_g}{T_g} - \frac{P_a}{T_a} = 1, \tag{B.6}$$

Eq. (B.5) simplifies to

$$B = gV_g\rho_a\left(1 - \frac{M_g}{M_a}\right). \tag{B.7}$$

In ballooning, the terms *superpressure* and *supertemperature* are often introduced (see [7, Section II]). Superpressure is defined to be

$$\Pi = P_g - P_a$$

and supertemperature is defined to be

$$\Theta = T_g - T_a.$$

In this case, Eq. (B.5) can be expressed in the form,

$$B = gV_g\rho_a\left(1 - \frac{(P_a+\Pi)T_aM_g}{P_a(T_a+\Theta)M_a}\right). \tag{B.8}$$

To determine the buoyancy b of a unit volume of gas in air, we can divide B by V_g and obtain,

$$b = g\rho_a\left(1 - \frac{M_g}{M_a}\right) \tag{B.9}$$

or the more general expression,

$$b = g\rho_a\left(1 - \frac{(P_a+\Pi)T_aM_g}{P_a(T_a+\Theta)M_a}\right). \tag{B.10}$$

From Eq. (B.10), we see that $b = b(\rho_a, T_a, \Pi, \Theta, M_g, M_a)$,

Appendix C

U.S. Standard Atmosphere

The U. S. standard atmosphere layers are presented in [9, pg. 15]. Data is available on eight layers. For each layer, a base layer altitude and top layer altitude is given with corresponding values for temperature, pressure, and density. Properties and assumptions are listed in [9, pg. 7]. In the following, H is the geopotential height and Z is the geometric height. Within each layer, the temperature is assumed to vary linearly from the base of the layer to the top of the layer, i.e.,

$$T_a = T_{B,i} + L'_i(H - H_{B,i}, \quad H_i \leq H \leq H_{i+1}, \tag{C.1}$$

where $T_{B,i}$ is the temperature at the base of the ith layer, H_i is the base of layer i (the top of layer $i-1$), and $L'_i = dT/dH$ in layer i. From [9, Eq. (12)], we have $dP_a = -g_0 \rho_a dH$

$$dH = -\frac{R}{g_0 M_a}\frac{T_a}{P_a} dP_a. \tag{C.2}$$

From Eq. (C.1) and Eq. (C.2), we have

$$\frac{dH}{T_B + L'(H - H_B)} = -\frac{R}{g_0 M_a}\frac{dP_a}{P_a}, \tag{C.3}$$

which can be integrated to yield the height as a function of P_a, i.e.,

$$H = \begin{cases} H_B + \dfrac{RT_B}{g_0 M_a} \ln \dfrac{P_b}{P_a}, & L' = 0, \\ H_B + \dfrac{T_B}{L'}\left[\left(\dfrac{P_B}{P_a}\right)^{(L'R)/(g_0 M_a)} - 1\right], & L' \neq 0. \end{cases} \tag{C.4}$$

The density of air ρ_a is a function of geopotential height where

$$\rho_a(H) = \frac{P_a(H) M_a}{R T_a(H)}, \tag{C.5}$$

Table C.1: Physical constants for standard atmosphere

Quantity	Value
Sea level air density	1.2250 kg/m^3
Sea level temperature	15° C = 288.15° K
Sea level pressure	9.80665 m/sec^2
Sea level molecular weight	28.9644 kg/kg-mol
Sea level molecular helium	28.9644 kg/kg-mol
Sea level molecular hydrogen	2.0159 kg/kg-mol
Sea level molecular ammonia	4.0026 kg/kg-mol
Universal gas constant	8314.32 J/°K(kg-mol)

and P_a, H, and T_a are related by Eqs. (C.1) and (C.4). Related parameters needed to calculate atmospheric properties are given in Table C.1. Assuming a standard atmosphere, the buoyancy is given by Eq. (B.9) (or Eq. (B.10)), where $\rho_a(H)$ is given by Eq. (C.5), T_a is given by Eq. (C.1), and H and P_a are related by Eq. (C.4).